*J. Fluid Mech.* (2018), *vol.* 844, *pp.* 5–35. © Cambridge University Press 2018 
doi:10.1017/jfm.2018.193

# Outer scales and parameters of adverse-pressure-gradient turbulent boundary layers

**Yvan Maciel[1,†], Tie Wei[2], Ayse G. Gungor[3] and Mark P. Simens[4]**

[1]Department of Mechanical Engineering, Laval University, Quebec City, QC, G1V 0A6 Canada

[2]Department of Mechanical Engineering, New Mexico Institute of Mining and Technology, Socorro, NM 87801, USA

[3]Faculty of Aeronautics and Astronautics, Istanbul Technical University, 34469 Maslak, Istanbul, Turkey

[4]School of Aeronautics, Universidad Politécnica de Madrid, 28040 Madrid, Spain

(Received 9 November 2017; revised 21 February 2018; accepted 22 February 2018; first published online 3 April 2018)

A clear and consistent framework for the analysis of the outer region of adverse-pressure-gradient turbulent boundary layers is established in this paper based on basic principles and theory, and the help of six adverse-pressure-gradient turbulent boundary layer databases and a zero-pressure-gradient one. Outer velocity and length scales for the mean velocity defect and the Reynolds stresses are discussed first. The conditions of validity of four velocity scales are determined in terms of the shape factor, since one scale is restricted to small velocity-defect boundary layers (the friction velocity $u_\tau$), one to large-defect ones (the pressure-gradient velocity $U_{po}$), while the two others are proper scales for all velocity-defect conditions (the Zagarola–Smits velocity $U_{zs}$ and the mixing-layer-type velocity $U_m$). The turbulent boundary layer equations are then used to bring out, in a consistent manner and without assuming any self-similar behaviour, a set of non-dimensional parameters characterizing the outer region of turbulent boundary layers with arbitrary pressure gradients. In terms of a generic outer length scale $L_o$ and velocity scale $U_o$, these non-dimensional parameters are the pressure-gradient parameter $\beta_o = L_o/(\rho U_o^2)\,\mathrm{d}p_e/\mathrm{d}x$, the Reynolds number $Re_o = U_o L_o/\nu(U_o/U_e)$ and the inertial parameter $\alpha_o = U_e V_e/U_o^2$, where $U_e$ and $V_e$ are respectively the streamwise and wall-normal components of mean velocity at the boundary layer edge. These parameters have a clear physical meaning: they are ratios of the order of magnitude of forces, with the Reynolds shear stress gradient (apparent turbulent force) as the reference force – inertial to apparent turbulent forces for $\alpha_o$, pressure to apparent turbulent forces for $\beta_o$ and apparent turbulent to viscous forces for $Re_o$. We discuss at length their significance and determine under what conditions they retain their meaning depending on the outer velocity scale that is considered. The seven boundary layer databases are analysed and compared using the established framework. An astonishing and impressive result is obtained: by choosing $U_o = U_{zs}$, the streamwise evolution of the three ratios of forces in the outer region can be accurately followed with $\beta_{zs}$, $\alpha_{zs}$ and $Re_{zs}$ in all these flows – not just the order of magnitude of these ratios. This cannot be achieved with $u_\tau$ and $U_{po}$, and only imperfectly with $U_m$. Consequently, $\beta_{zs}$, $\alpha_{zs}$ and $Re_{zs}$ can

† Email address for correspondence: yvan.maciel@gmc.ulaval.ca

https://doi.org/10.1017/jfm.2018.193 Published online by Cambridge University Press

be used to follow – in a global sense – the streamwise evolution of the streamwise mean momentum balance in the outer region.

**Key words:** turbulent boundary layers, turbulent flows

## 1. Introduction

Rooted in the works of Prandtl and von Kármán, the initial theoretical concepts behind turbulent boundary layers (TBLs) influenced by pressure gradients were developed mostly in the 1950s by Rotta (1950), Clauser (1954, 1956), Coles (1956) and Townsend (1956*a*,*b*) among others. At the time, these concepts were tested usually only with the experimental datasets at high Reynolds numbers of Ludwieg & Tillmann (1949) and Clauser (1954). The most comprehensive ensemble of data, with six adverse-pressure-gradient (APG) TBL datasets, was used by Coles (1956) to test his defect law called the law of the wake. However, a full validation and improvement of the various theories was not possible since these datasets did not include accurate near-wall velocity and wall shear stress data. Furthermore, the range of flow conditions was limited.

In the 1960s, Townsend (1961), Perry, Bell & Joubert (1966) and McDonald (1969) proposed modifications or extensions to the classical law of the wall, while Mellor & Gibson (1966) revisited the theory behind equilibrium TBLs. Efforts were also put on the advancement of boundary layer computational methods and they culminated in the important Stanford conference of 1968 (Coles & Hirst 1969; Kline, Coles & Hirst 1969). In one of the conference papers, Coles (1969) indicated that the data were not entirely sufficient in terms of scope and quality. Despite the repeated mention of 'an important continuing need for more accurate and extensive experimental data' during the conference, experiments on TBLs under pressure gradients were scarce after the 1960s. A few experiments were nonetheless conducted. They are briefly presented in Maciel, Rossignol & Lemay (2006*a*). Direct numerical simulations (DNS) of APG TBLs started to appear in the 1990s with those of Spalart & Watmuff (1993) and Na & Moin (1998), followed by that of Skote & Henningson (2002). On the theoretical front, new or modified theories for TBLs with pressure gradients were developed based on asymptotic analysis (Yajnik 1970; Afzal 1983; Melnik 1989; Durbin & Belcher 1992; Afzal 2008) or dimensional/similarity analysis (Perry & Schofield 1973; Kader & Yaglom 1978; Skote & Henningson 2002; Maciel, Rossignol & Lemay 2006*b*).

Nowadays, we see a resurgence in popularity of research on APG TBLs, which is more than welcome in view of the importance of APG flows in nature and industry. Detailed experimental and numerical databases are being produced by several research groups. In the case of fairly low-Reynolds-number studies, these include the experiments of Angele & Muhammad-Klingmann (2006), Indinger, Buschmann & Gad-el Hak (2006), Maciel *et al.* (2006*a*), Rahgozar & Maciel (2012), Harun *et al.* (2013) and Knopp *et al.* (2015), the DNS of Marquillie, Laval & Dolganov (2008), Lee & Sung (2009), Gungor *et al.* (2016) and Hosseini *et al.* (2016), and the well-resolved large-eddy simulations (LES) of Hickel & Adams (2008), Inoue *et al.* (2013), Bobke *et al.* (2017) and Sato *et al.* (2017). However, to test and improve the near-wall similarity laws and layer-structure models, high-quality near-wall data at higher Reynolds numbers and covering a wide spectrum of pressure-gradient

https://doi.org/10.1017/jfm.2018.193 Published online by Cambridge University Press

conditions are needed. Fortunately, such data are starting to appear both experimentally and numerically. On the experimental side, large-scale APG TBLs have been extensively measured with high-resolution particle image velocimetry and particle tracking velocimetry by Cuvier *et al.* (2017) and Knopp *et al.* (2017), with $Re_\theta$ reaching 41 000 and 23 000, respectively ($Re_\theta$ is defined in § 2). Two recent DNS have also reached relatively high Reynolds numbers, although not as high as those of the aforementioned experiments. They are the DNS of a strongly decelerating TBL of Gungor *et al.* (2017) with $Re_\theta$ reaching 8000, and the APG TBL of Kitsios *et al.* (2017) with a near-equilibrium region from $Re_\theta = 10\,000$ to 12 300, and $\beta_{RC} \approx 39$ ($\beta_{RC}$ is the Rotta–Clauser pressure-gradient parameter presented in § 2).

Despite the theoretical works cited above, the theory behind APG TBLs is far from being as mature as that for canonical turbulent wall flows. Validation of the various theoretical propositions is still necessary and, consequently, the analysis of the newly produced databases still does not rest on thoroughly validated theoretical foundations. In terms of similarity laws, we still do not know under what conditions of pressure-gradient parameter (which one?), Reynolds number (which one?) and upstream history (how to formalize it mathematically?) the classical law of the wall loses its validity for large-defect TBLs. There is no consensus either on the similarity laws that should replace the classical law of the wall, or on the layer structure of large-defect TBLs.

Furthermore, no agreement exists on the scales and non-dimensional parameters that should be used, which is the focus of the present paper. An illustration of this is the fact that the scales and parameters used in past and recent studies differ considerably from one study to another. There exist indeed a multitude of scales and non-dimensional parameters that can be used for APG TBLs, but a consistent set of these parameters and scales has yet to be defined. For example, researchers commonly use the Rotta–Clauser pressure-gradient parameter $\beta_{RC}$ and the Reynolds number $Re_\theta$ (both defined below) to analyse APG TBLs – the reason being that these non-dimensional parameters have been used frequently in the past. However, it can be shown that $\beta_{RC}$ and $Re_\theta$ do not form a consistent set of parameters. In other words, they do not appear together in the non-dimensional form of the boundary layer equations simply because they are not defined with the same length and velocity scales. Furthermore, the exact physical meaning of these parameters is not clear – this is clarified in the present paper.

We do not consider in this study the near-wall region and its related similarity laws because, as stated above, there are not enough high-quality near-wall data at high Reynolds number for APG TBLs in the literature. For instance, it cannot be done with the six APG databases used here. The Reynolds number is too low for five of them and the two experimental databases do not include detailed near-wall data. For this reason, we focus our attention on the outer region of APG TBLs. However, a widely accepted wall-normal layer structure does not exist in the case of large-defect TBLs. Consequently, there is no precise definition of what constitutes the outer region in these cases. In this study, we have decided to consider the lower limit of the outer region as the approximate height where the viscous stress gradient is negligible with respect to the Reynolds shear stress gradient. This lower limit corresponds approximately to $y = 0.15\delta$ for the flows studied here, where $\delta$ is the boundary layer thickness defined in the present paper as the wall-normal position where $U = 0.99U_e$.

The two main goals of the paper are to establish a clear and consistent framework for the analysis of the outer region of APG TBLs and, based on this framework, to perform such an analysis using six APG TBL databases and a zero-pressure-gradient

https://doi.org/10.1017/jfm.2018.193 Published online by Cambridge University Press

| Flow | $Re_\theta$ | $C_f \times 10^3$ | $\beta_{RC}$ | $H$ | $G$ |
|---|---|---|---|---|---|
| ZPG SJM | 2900–6155 | 3.32–2.73 | 0 | 1.38–1.36 | 6.76–7.26 |
| SK | 39 120–50 890 | 0.59–0.55 | 19.9–21.2 | 2.01–1.99 | 29.2–30.2 |
| MRL | 3355–12 690 | 2.27–0.00 | 3.20–$\infty$ | 1.72–3.85 | 12.5–$\infty$ |
| Hickel | 712–5270 | 5.17–0.00 | 0.21–$\infty$ | 1.45–3.31 | 6.12–$\infty$ |
| NACA4412 | 825–2810 | 3.97–0.22 | 0.65–85.0 | 1.59–2.74 | 8.34–60.9 |
| DNS2015 | 1325–3915 | 3.57–0.00 | 1.61–$\infty$ | 1.49–3.43 | 7.85–$\infty$ |
| DNS2017 | 1685–7460 | 3.70–0.21 | 0.61–78.3 | 1.42–3.01 | 6.91–65.8 |

TABLE 1. Ranges of common boundary layer parameters for the databases used in the present paper. The ranges cover only the selected regions of each flow, and are expressed in order of streamwise evolution. See text for references.

(ZPG) one. Using these databases, we first determine proper outer velocity and length scales for small to large momentum-defect boundary layers, and under what conditions they should be used. Consistent sets of non-dimensional parameters governing the outer region are then obtained directly from the TBL equations, without assuming any type of self-similar behaviour. Finally, the outer region of the different APG TBLs is analysed using these consistent sets of non-dimensional parameters and scales, and the physical meaning of the non-dimensional parameters is discussed at length. It is shown that these non-dimensional parameters have a clear physical meaning, which is not the case for the most commonly used non-dimensional parameters $\beta_{RC}$ and $Re_\theta$.

## 2. Databases

We use seven databases to test our ideas on the characterization of the outer region of APG TBLs. These databases were chosen based on two criteria: $Re_\theta$ at least above 1000 in most of the flow, and accurate data of all Reynolds stresses (except $\langle w'^2 \rangle$ for the experimental databases). We also wanted non-equilibrium APG TBLs covering small to very large velocity-defect conditions. Five of the databases are of this type. They all correspond to decelerated TBLs where the velocity defect keeps increasing, leading to flow separation in three cases. They include the experiments of Maciel *et al.* (2006*a*) (MRL), the well-resolved LES of Hickel & Adams (2008) (Hickel) as well as the recent DNS of Gungor *et al.* (2016) (DNS2015), Gungor *et al.* (2017) (DNS2017) and Hosseini *et al.* (2016) (NACA4412). The latter is a DNS of the flow around the asymmetric NACA4412 wing section at an angle of attack of 5 degrees and a chord Reynolds number of 400 000. The other two databases are the DNS of a ZPG TBL at high Reynolds number of Sillero, Jiménez & Moser (2013) (ZPG SJM) and the experiments of Skåre & Krogstad (1994) (SK) of a large-defect APG TBL in near equilibrium.

Table 1 presents commonly used boundary layer non-dimensional parameters for these different flows, while figure 1 compares the streamwise evolutions of these parameters. Such a comparison between different APG flows can only be done if $x$ is normalized with a proper reference length $L_x$. Determining such a reference length is not a trivial issue. The theoretical analysis presented in § 4 reveals that one candidate is $L_x = (U_e/V_e)\delta$. However, using a reference length that implicitly depends on the variable being normalized, $x$, is not desirable nor practicable. Furthermore, the normalized variable $x/L_x$ would become strongly dependent on the pressure gradient, making the problem circular. For strong pressure gradients, using $L_x = (U_e/V_e)\delta$

https://doi.org/10.1017/jfm.2018.193 Published online by Cambridge University Press

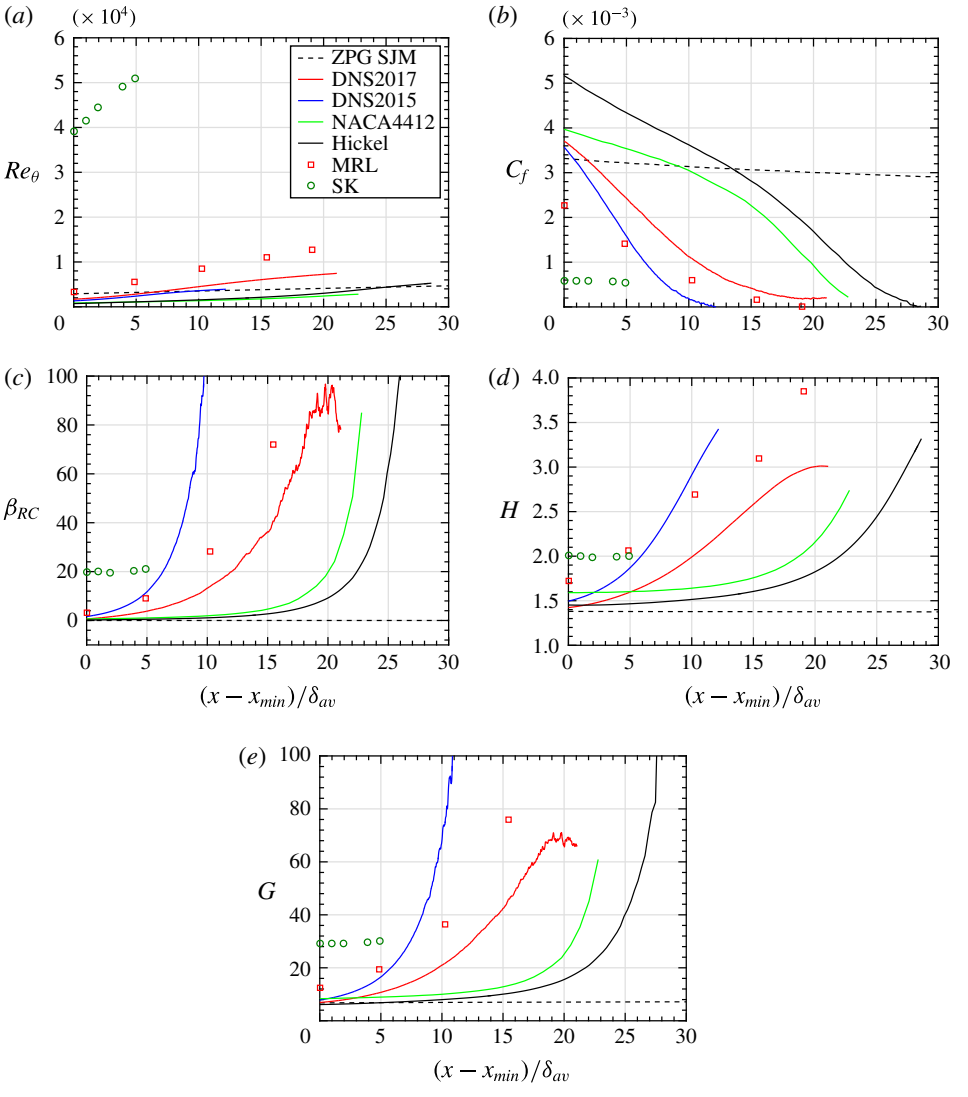



FIGURE 1. (Colour online) Streamwise evolution of commonly used boundary layer non-dimensional parameters for the selected regions of the seven flows. Only the first half of the region is shown for ZPG SJM.

or $L_x = \delta$ can even lead to the absurd situation where $x/L_x$ starts decreasing as $x$ increases. After considering different possibilities, we have determined that a good choice of streamwise reference length is the average value of $\delta$ over the $x$ range considered for the given flow, which we name $\delta_{av}$. In other words, $\delta_{av}$ is the average size of the boundary layer in the flow region considered. We therefore use in the present paper $L_x = \delta_{av}$.

To compute the non-dimensional parameters presented in table 1 and figure 1, $U_e$ and $\delta$ have to be determined first. Note however that the traditional definitions of $U_e$ and $\delta$ become ill-defined in flows where the external inviscid velocity increases with $y$. Such a situation is encountered in many flows with curvature or variable divergence

https://doi.org/10.1017/jfm.2018.193 Published online by Cambridge University Press

of the mean streamlines, such as flows around an airfoil, like NACA4412. A few alternatives have been proposed in the literature to circumvent this problem (Spalart & Watmuff 1993; Vinuesa *et al.* 2016). In the present study, this situation is encountered for the Hickel flow and in a downstream section of flow NACA4412. In these cases, the wall-normal position of $U_e$ is the position where the mean spanwise vorticity levels off to a low value. Such a position is easily detected in these two flows because they were obtained numerically with sufficient spatial resolution. In flows DNS2015 and DNS2017, the external velocity decreases with $y$. In these cases, $U_e$ is defined as the maximum $U$ along $y$. In all flows, $\delta$ is the $y$ position where $U = 0.99U_e$, as already mentioned above. It should be kept in mind that, since we are not studying similarity laws, high accuracy in the determination of $\delta$ and $U_e$ is not required. All integral thicknesses discussed below are obtained by integrating up to $y = \delta$.

In figure 1, the streamwise positions shown for the experimental MRL database cover all available data up to separation. In the case of SK, the five stations are in the quasi-equilibrium range of the flow. For the three simulations performed in rectangular boxes (Hickel, DNS2015, DNS2017), the regions were selected based on two criteria: first point sufficiently far from the inlet plane, and last point at separation or sufficiently far from the outlet plane. In the case of NACA4412, the region selected, on the suction side, is from 0.458 chord from the leading edge (far enough from the transition point at 0.1 chord) up to the trailing edge. Finally, $x_{min}$ is the $x$ coordinate of the first point.

Figure 1($a$) presents the distributions of the local boundary layer Reynolds number $Re_\theta = U_e\theta/\nu$ for the different flows, where $U_e$ is the streamwise velocity at the boundary layer edge, $\theta$ is the momentum thickness and $\nu$ is the kinematic viscosity. It can be seen from these distributions of $Re_\theta$ that the SK flow is at a much higher Reynolds number than the other flows. In comparison to the ZPG TBL, $Re_\theta$ increases more rapidly in the other flows because of the sustained APG. Note however that we show in § 5 that $Re_\theta$ should normally represent the local ratio of apparent turbulent forces to viscous forces in the outer region, but that it fails to do it.

Figure 1($b$) shows the skin friction coefficient $C_f = 2\tau_w/(\rho U_e^2)$, where $\tau_w$ is the wall shear stress (skin friction) and $\rho$ is the density. The $C_f$ evolutions are quite different for these flows. The initial values of $C_f$ depend on the type of upstream effects before $x_{min}$ (pressure gradient, curvature, initial conditions) and on the local Reynolds number. Coefficient $C_f$ decreases slowly for the two quasi-equilibrium flows, namely the ZPG TBL and SK flow. The decrease in these cases is mainly due to the increasing Reynolds number (see figure 1$a$). In contrast, the $C_f$ decrease is important for the non-equilibrium APG TBLs. Three of the flows eventually separate ($C_f = 0$), whereas NACA4412 and DNS2017 approach separation but never reach it.

In the following discussion, the change from small to large mean velocity defect is expressed with both the shape factor $H = \delta^*/\theta$, where $\delta^*$ is the displacement thickness, and the Rotta–Clauser pressure-gradient parameter $\beta_{RC}$, which is an outer pressure-gradient parameter:

$$\beta_{RC} = \frac{\delta^*}{\tau_w}\frac{\mathrm{d}p_e}{\mathrm{d}x} = -\frac{\Delta}{u_\tau}\frac{\mathrm{d}U_e}{\mathrm{d}x} = \left(\frac{U_{po}}{u_\tau}\right)^2. \tag{2.1}$$

Note that the pressure at the edge of the boundary layer $p_e$ is used since we are interested here in the outer region. In this manner, we can also express $\beta_{RC}$ with the edge velocity gradient as done in the second form shown in (2.1), where $\Delta$ is a defect displacement thickness defined in table 2, and also known as the Rotta–Clauser length

https://doi.org/10.1017/jfm.2018.193 Published online by Cambridge University Press

| Condition of validity | Outer velocity scale | Related defect displacement thickness |
|---|---|---|
| Small defect<br>$\beta_{RC} < 8$<br>$H < 1.8$ | $u_\tau = \left(\dfrac{\tau_w}{\rho}\right)^{1/2}$ | $\Delta = \displaystyle\int_0^\delta \frac{U_e - U}{u_\tau}\,\mathrm{d}y = \delta^* \frac{U_e}{u_\tau}$ |
| Large defect<br>$\beta_{RC} > 8$<br>$H > 1.8$ | $U_{po} = u_\tau \beta_{RC}^{1/2} = \left(\dfrac{\delta^*}{\rho}\dfrac{\mathrm{d}p_e}{\mathrm{d}x}\right)^{1/2}$ | $\delta_{po} = \displaystyle\int_0^\delta \frac{U_e - U}{U_{po}}\,\mathrm{d}y = \delta^* \frac{U_e}{U_{po}} = \frac{\Delta}{\beta_{RC}^{1/2}}$ |
| All defects<br>All $\beta_{RC}$ and $H$ | $U_{zs} = U_e \dfrac{\delta^*}{\delta}$ | $\delta = \displaystyle\int_0^\delta \frac{U_e - U}{U_{zs}}\,\mathrm{d}y$ |
| All defects<br>All $\beta_{RC}$ and $H$ | $U_m = 2[U_e - U(y = 0.5\delta)]$ | $\delta_m = \displaystyle\int_0^\delta \frac{U_e - U}{U_m}\,\mathrm{d}y = \delta^* \frac{U_e}{U_m}$ |

TABLE 2. Velocity and length scales for the outer region. The conditions of validity expressed in terms of inequalities are for the scaling of the Reynolds stresses only, and they are approximate since they depend on Reynolds number and upstream history.

scale (Rotta 1950; Clauser 1954). The last form, $(U_{po}/u_\tau)^2$, shows that $\beta_{RC}$ is related to the ratio of pertinent outer velocity scales. These velocity scales and the physical significance of $\beta_{RC}$ and $H$ are discussed at length in the following sections.

The evolutions of $\beta_{RC}$ and $H$ are shown respectively in figures 1(*c*) and 1(*d*). Note that $\beta_{RC}$ is null in the case of the ZPG TBL and tends to infinity when $u_\tau$ (or $\tau_w$) tends to zero, which happens at the downstream end of flows MRL, DNS2015 and Hickel. The values of $C_f$, $\beta_{RC}$ and $H$ should be constant for flows with self-similar velocity profiles, i.e. equilibrium TBLs (Rotta 1950; Maciel *et al.* 2006*b*). Of the six APG TBLs considered here, the only one that approaches such a condition is SK, which was designed to be an equilibrium TBL. The other five APG TBLs exhibit steady increases of $\beta_{RC}$ and $H$ in the flow zones considered, except for the beginning of Hickel and the end of DNS2017. These increases indicate that these are disequilibrium TBLs with increasing momentum defect. The mean velocity profiles of figure 2 show the increase of momentum defect in the case of DNS2017. The trend is qualitatively similar for the other four non-equilibrium APG TBLs. All five non-equilibrium APG TBLs present regions of rapid increase of $\beta_{RC}$ and $H$. They can all be considered as flows with strong disequilibrium conditions.

We also present in figure 1(*e*) the defect shape factor

$$G = \int_0^\delta \left(\frac{U_e - U}{u_\tau}\right)^2 \mathrm{d}y \Big/ \int_0^\delta \frac{U_e - U}{u_\tau}\,\mathrm{d}y = \frac{U_e}{u_\tau}\left[1 - \frac{1}{H}\right]. \tag{2.2}$$

This was introduced by Rotta (1950) to analyse TBLs in arbitrary pressure distributions and four years later by Clauser (1954) in his study of equilibrium APG TBLs. Like $H$ and $\beta_{RC}$, $G$ increases with increasing velocity defect. According to Clauser (1954) and Mellor & Gibson (1966), $G$ is less dependent on the Reynolds number (or $u_\tau/U_e$) than $H$ in the case of equilibrium TBLs. However, as opposed to $H$ but similarly to $\beta_{RC}$, $G$ does not remain finite at separation or reattachment, when $u_\tau$ is zero. This is the reason why the last portions of flows MRL, DNS2015 and Hickel do not appear in figure 1(*e*).

https://doi.org/10.1017/jfm.2018.193 Published online by Cambridge University Press

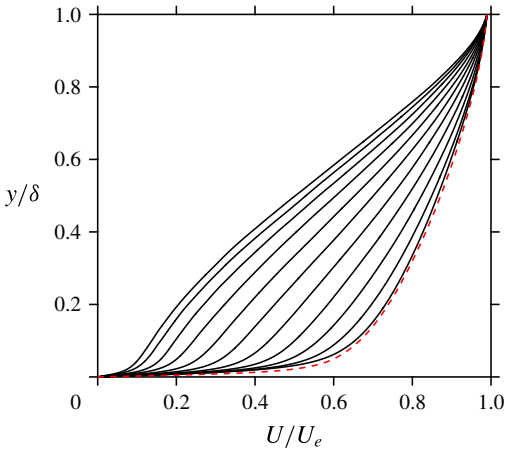



FIGURE 2. (Colour online) Equidistant mean velocity profiles of DNS2017 spanning the selected streamwise region shown in figure 1 (solid lines), and of ZPG SJM at $Re_\theta = 2900$ (dashed red line).

## 3. Velocity and length scales of the outer region

We demonstrate in this section that the velocity and length scales shown in table 2 are pertinent scales for the mean velocity defect and the Reynolds stresses in the outer region of APG TBLs. We also determine under what precise conditions they can be considered proper scales, since some scales are restricted to small-defect TBLs ($u_\tau$, $\Delta$) or large-defect TBLs ($U_{po}$, $\delta_{po}$), while the others are proper scales for all velocity-defect conditions ($U_{zs}$, $\delta$; $U_m$, $\delta_m$). It is important to stress that the scales studied here are not the only ones possible. They have been chosen because they are theoretically valid and this validity has been confirmed in the past with solid empirical evidence.

As stated at the end of the introduction, there is no precise definition of the outer region in the case of large-defect APG TBLs. In this study, the lower limit of the outer region is taken as the approximate height where the viscous stress gradient is negligible with respect to the Reynolds shear stress gradient. For the flows studied here, this lower limit corresponds approximately to $y = 0.15\delta$.

Since the velocity scales presented in table 2 are scales of the mean velocity defect in the outer region, it is logical to use the corresponding defect displacement thickness as the length scale. These are indeed the outer length scales shown in table 2. The advantage of defect displacement thicknesses is that they are independent of Reynolds number and roughness in the case of equilibrium TBLs (Clauser 1954), which is also the case of $\delta$ (since it is also a defect displacement thickness, as seen in table 2) but not of $\delta^*$ and $\theta$. In the case of equilibrium TBLs, it is easy to show that $\delta^*/\delta$ and $\theta/\delta$ tend to zero like $C_f^{1/2}$ ($u_\tau/U_e$) as the Reynolds number tends to infinity. Therefore, $\delta^*$ and $\theta$ are not appropriate outer length scales.

However, there is no obligation to stick to the pairs shown in table 2, firstly, because the velocity scales scale not only the mean velocity defect but also the Reynolds stresses, and secondly, because what matters is that the length scale follows the magnitude change of the outer region thickness under all conditions. In the following, we generally use the boundary layer thickness $\delta$ as the outer length scale because it simplifies the analysis of the data.

https://doi.org/10.1017/jfm.2018.193 Published online by Cambridge University Press

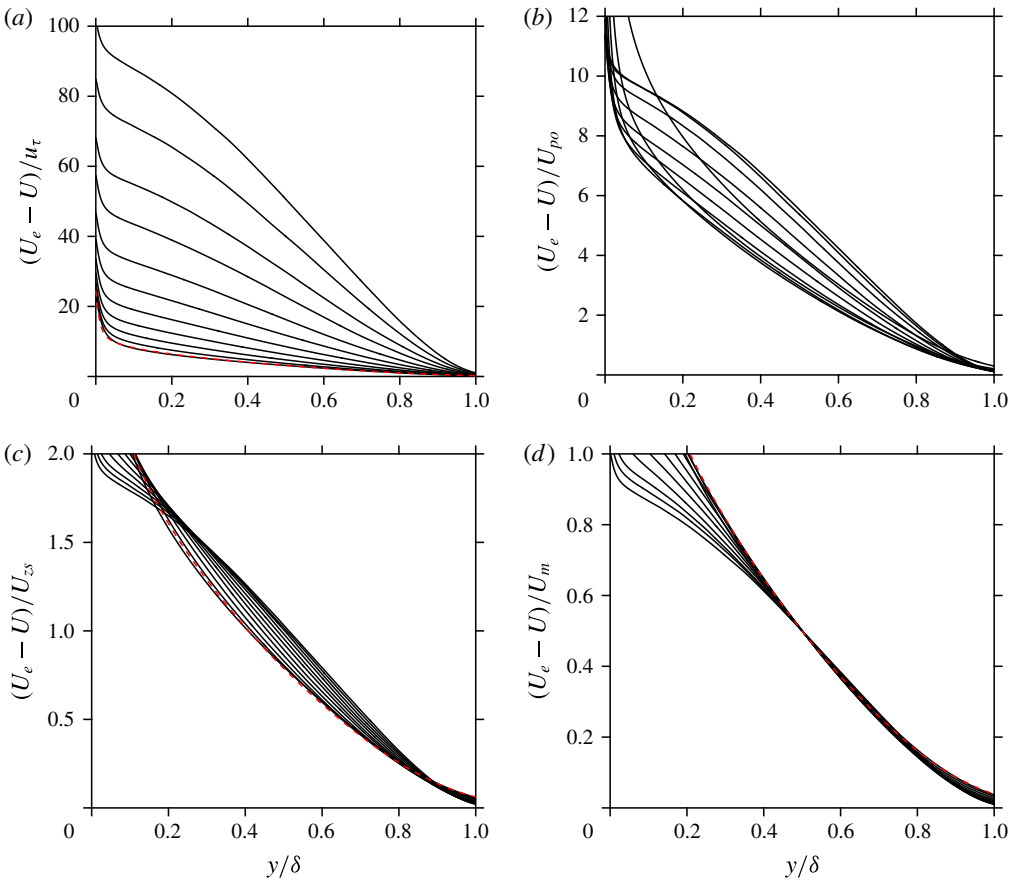



FIGURE 3. (Colour online) Mean velocity-defect profiles for the same 11 positions of DNS2017 as in figure 2 (solid lines) and for ZPG SJM at $Re_\theta = 2900$ (dashed red line). Normalized with (*a*) $u_\tau$, (*b*) $U_{po}$, (*c*) $U_{zs}$ and (*d*) $U_m$.

Figure 3 shows the mean velocity defect normalized by the four velocity scales presented in table 2 in the case of the flow DNS2017 and the ZPG TBL of SJM. The same positions as in figure 2 are used. The trends seen in figure 3 as the velocity defect increases are qualitatively similar for the four other non-equilibrium APG TBLs. It is important to mention that in the case of non-equilibrium APG TBLs, we do not expect to find self-similar behaviour in the outer region or, even less, a universal outer behaviour common to all non-equilibrium flows. Therefore, in the context of non-equilibrium APG TBLs, a scale should always reflect the order of magnitude of the scaled variable, but it is not required that it reveals scale invariance – that it 'collapses profiles' of the scaled variable. The four plots of figure 3 clearly show that such a collapse is not possible. No velocity scale will be able to reveal self-similarity or universal similarity since the shape of the mean velocity-defect profile in the outer region varies as a function of local conditions and upstream history. Self-similarity of the mean velocity-defect profile in the outer region is expected only in the case of equilibrium TBLs (Rotta 1950; Clauser 1954), which can only be truly achieved when approaching an infinite Reynolds number (Rotta 1950; Maciel *et al.* 2006*b*).

https://doi.org/10.1017/jfm.2018.193 Published online by Cambridge University Press

The friction velocity $u_\tau$ is the outer velocity scale generally used for canonical wall flows (ZPG TBL, pipe and channel flows) and for small-defect pressure-gradient TBLs (both favourable- and adverse-pressure-gradient cases). In the latter case, the outer length scale used in combination with $u_\tau$ is usually $\delta$ or $\Delta$. For large mean velocity defect (large $\beta_{RC}$ and $H$), it is known that $u_\tau$ and $\Delta$ are no longer proper outer scales. Figure 3(*a*) illustrates this point for $u_\tau$. The mean velocity defect normalized with $u_\tau$ increases by one order of magnitude with a change of shape factor $H$ from 1.4 to 3.0. The situation is even worse for flows that separate, such as MRL, DNS2015 and Hickel, since the mean velocity defect normalized with $u_\tau$ tends to infinity at separation. Nonetheless, the five non-equilibrium TBLs studied here indicate that $u_\tau$ can be considered a scale of the mean velocity defect up to about $H = 1.8$. In the case of the DNS2017 profiles shown in figure 3(*a*), this corresponds to the five lower profiles. For $H < 1.8$, the order of magnitude of the mean velocity defect normalized with $u_\tau$ is 10 for all TBLs.

For large mean velocity-defect TBLs, Mellor & Gibson (1966) proposed $U_{po}$ and $\delta_{po}$, where the index $p$ stands for pressure and $o$ for outer region. As can be seen with the equations in table 2, these scales were obtained directly by a transformation of the traditional scales for small $\beta_{RC}$, namely $u_\tau$ and $\Delta$, by using the factor $\beta_{RC}^{1/2}$. Figure 3(*b*) shows that $U_{po}$ can scale all the mean velocity-defect profiles of DNS2017, with an order of magnitude of 10, and this is also the case for all the other APG TBLs. However, $U_{po}$ cannot be used for ZPG TBLs since it is null in this case. It cannot be used either for cases or flow regions where $\mathrm{d}p_e/\mathrm{d}x$ is close to zero.

Figures 3(*c*) and 3(*d*) show that the Zagarola–Smits velocity scale $U_{zs}$ and the mixing-layer-type velocity scale $U_m$ scale the mean velocity defect in all defect conditions, leading to an order of magnitude of one of the scaled defect. This has already been demonstrated in the past by Maciel *et al.* (2006*b*) and Logdberg, Angele & Alfredsson (2008) in the case of $U_{zs}$ and by Gungor *et al.* (2014) and Gungor *et al.* (2016) in the case of $U_m$. Gungor *et al.* (2014) introduced $U_m$ in order to be able to compare the velocity statistics of APG TBLs with those of mixing layers. Indeed, $U_m$ is a velocity scale of the type used for mixing layers.

Although some readers might be tempted to see 'collapse of the profiles' in the case of $U_m$, it is not the case, and it is not the case for any of the other non-equilibrium APG TBLs. We emphasize that $U_m$ is not a 'better' outer velocity scale for the mean velocity defect than the others, since self-similarity or general scale invariance does not exist for non-equilibrium TBLs. Conversely, in the case of equilibrium APG TBLs, all the velocity scales of table 2 reveal self-similarity of the mean velocity-defect profile, except $u_\tau$ at separation and reattachment and $U_{po}$ for ZPG TBLs. This is simply because equilibrium APG TBLs are by definition in dynamic equilibrium in the outer region, and this dynamic equilibrium does not depend on any scale.

We now consider the outer scaling of the Reynolds stresses. Figure 4 shows $\langle u^2 \rangle$ normalized by the four velocity scales presented in table 2, for the same positions of DNS2017 and ZPG SJM as in figure 3. The abscissa has a logarithmic scale in order to reveal the near-wall behaviour. The scaling situation is similar to what was discussed for the mean velocity defect: $u_\tau$ scales $\langle u^2 \rangle$ only in the small-defect cases while the other three velocity scales work for all defect cases, except $U_{po}$, which cannot be used for cases where $\mathrm{d}p_e/\mathrm{d}x$ is zero or close to zero. The disappearance of the near-wall peak and the appearance of an outer peak as the defect increases can clearly be seen in all the plots of figure 4. The difference in position of the near-wall peaks of the ZPG TBL and of the first profile of DNS2017 is a Reynolds-number effect due to the fact that the outer length scale $\delta$ is used in these figures.

https://doi.org/10.1017/jfm.2018.193 Published online by Cambridge University Press

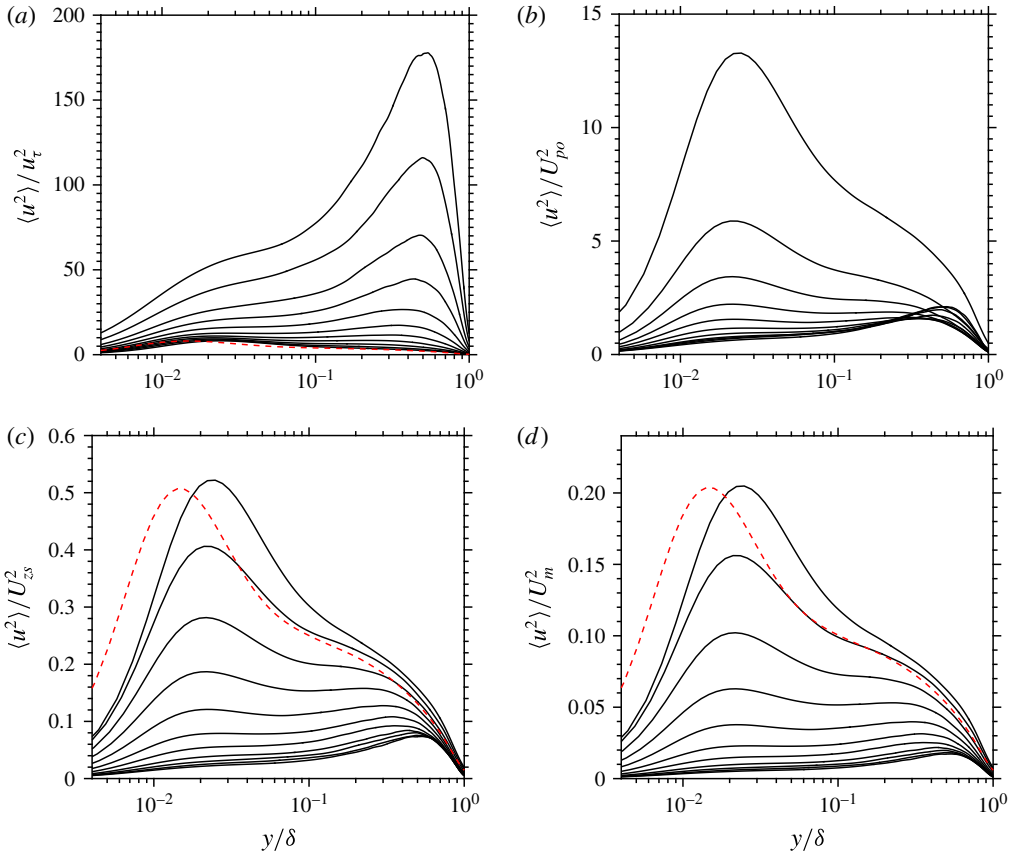



FIGURE 4. (Colour online) Semilog plots of $\langle u^2\rangle$ for the same 11 positions of DNS2017 as in figure 2 (solid lines) and for ZPG SJM at $Re_\theta = 2900$ (dashed red line). Normalized with (*a*) $u_\tau$, (*b*) $U_{po}$, (*c*) $U_{zs}$ and (*d*) $U_m$. Note that $U_{po} = 0$ for ZPG TBLs.

The evolution of the scaled $\langle u^2\rangle$ profiles with $H$ seen in figure 4 is qualitatively similar for the other four non-equilibrium APG TBLs. This observation is also true for the scaled profiles of the other components of the Reynolds stress tensor (see figures 5–9). For a given $H$ value, the presence of one or two peaks in the $\langle u^2\rangle$ profiles, the position of the outer peak (when it exists), and the amplitude of the scaled peaks is similar for all APG TBLs, including the quasi-equilibrium one of SK. This will be shown below.

Figure 5 shows the Reynolds shear stress normalized by the four velocity scales, again for the same positions of DNS2017 and ZPG SJM as in figure 3. The Reynolds shear stress profiles, like those of $\langle v^2\rangle$, have always only one maximum, as opposed to $\langle u^2\rangle$ and $\langle w^2\rangle$, whose near-wall maximum is distinct from the outer maximum. The maximum of the Reynolds shear stress moves away from the wall as $H$ increases. As expected, it can be seen that $u_\tau$ scales the Reynolds shear stress only when the velocity defect is small, while $U_{po}$ scales it when the defect is large. When the scaling is valid, $-\langle uv\rangle/u_\tau^2$ and $-\langle uv\rangle/U_{po}^2$ are of order of magnitude one. In contrast, for all types of TBLs, $-\langle uv\rangle/U_{zs}^2$ and $-\langle uv\rangle/U_m^2$ are of order of magnitude 0.1 and 0.01, respectively. We find the same orders of magnitude for all the flows studied here. The

https://doi.org/10.1017/jfm.2018.193 Published online by Cambridge University Press

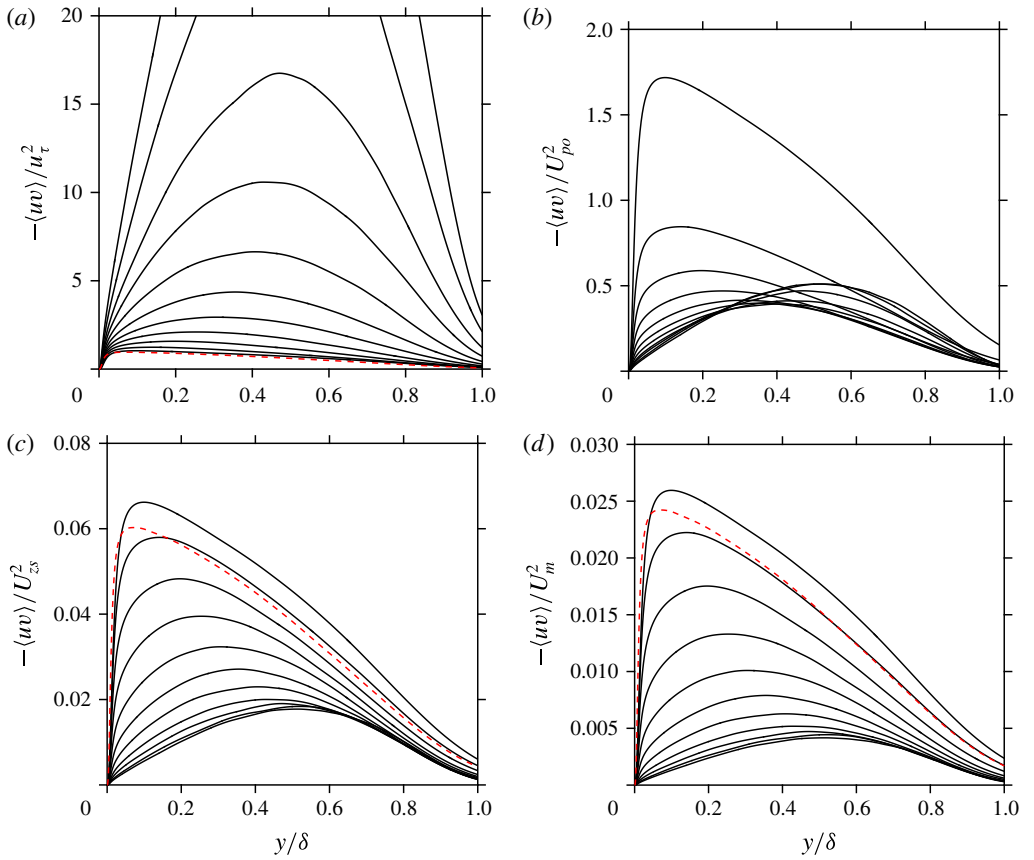



FIGURE 5. (Colour online) Reynolds shear stress for the same 11 positions of DNS2017 as in figure 2 (solid lines) and for ZPG SJM at $Re_\theta = 2900$ (dashed red line). Normalized with (*a*) $u_\tau$, (*b*) $U_{po}$, (*c*) $U_{zs}$ and (*d*) $U_m$. Note that $U_{po} = 0$ for ZPG TBLs.

order of magnitude of the scaled Reynolds shear stress is an important result for the analysis of the next section.

As an aside, it is interesting to note that Abe (2017) has found that the maximum Reynolds shear stress scales very well the root-mean-square value of the wall-pressure fluctuations throughout the APG zone and at the beginning of the separated zone in the case of turbulent separation bubbles. Wall-pressure fluctuations can therefore be strongly related to outer region motions.

The maxima of the Reynolds stress profiles will be used to demonstrate the scaling behaviour of all Reynolds stress components and for all flows. Beforehand, figure 6 shows how the wall-normal position of this maximum evolves as a function of $H$ and $\beta_{RC}$, in the case of $\langle u^2\rangle$. Although not unique, it is seen that the evolution of the wall-normal position is quite similar for all the flows. Firstly, the transition from a near-wall-peak maximum to an outer-peak maximum occurs in the range $H = 1.7$–$1.9$ ($\beta_{RC} = 5$–$9$). The wall-normal position of the outer-peak maximum then increases steadily and levels off around $0.5\delta$ for large $H$ (large $\beta_{RC}$). Because $\beta_{RC}$ varies from zero to infinity, it is not a practical indicator of the state of the boundary layer. This is seen in figure 6(*b*) where flows or flow regions with null or small $\mathrm{d}p_e/\mathrm{d}x$ ($\beta_{RC} < 1$) and close to separation (null or small $u_\tau$; $\beta_{RC} > 10^4$) cannot be shown. From now on,

https://doi.org/10.1017/jfm.2018.193 Published online by Cambridge University Press

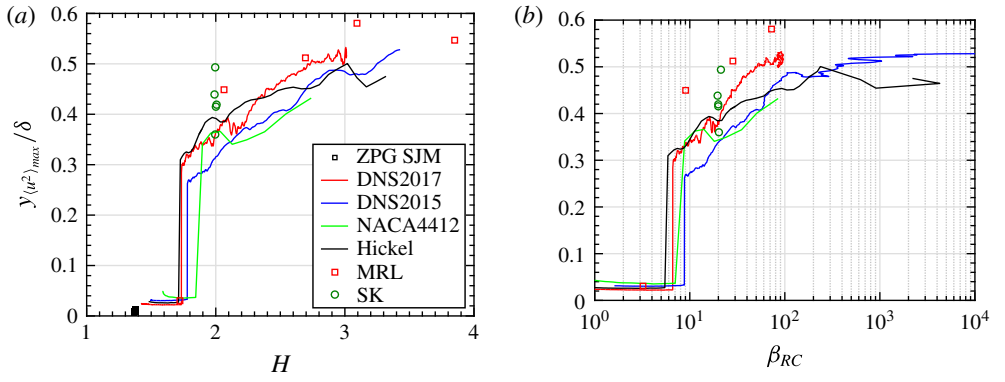



FIGURE 6. (Colour online) Wall-normal position of the maximum of $\langle u^2 \rangle$ as a function of (*a*) $H$ and (*b*) $\beta_{RC}$.

we will use only $H$ as an indicator of the extent of the mean velocity defect since it allows data near or at ZPG and near or at separation or reattachment to be shown.

Figure 7 shows the wall-normal position of the maximum of all Reynolds stress components as a function of $H$. In this figure, the wall-normal position is normalized by $\delta^*$ to show that $\delta^*$ indeed scales the position of the outer maximum of all Reynolds stresses (similar location for the four Reynolds stresses) for all flows and all defect cases when such an outer maximum exists. Kitsios *et al.* (2017) also noticed that the outer peak of all Reynolds stresses was located at $y = \delta^*$ in the case of a near-equilibrium APG TBL with $H = 2.35$. In the large-defect cases of the present flows, the outer peaks are in fact close to the position of the outermost inflection point of the mean velocity profile, as observed previously by Elsberry, Zhou & Wygnanski (2000) in a quasi-equilibrium large-defect APG TBL with $H \approx 2.45$. These authors suggested that their flow was dominated by a single inflectional instability occurring at the position of the outermost inflection point of the mean velocity profile. In the present five non-equilibrium APG TBLs, there are however upstream flow regions with smaller mean velocity defects (roughly for $H < 2$) where the Reynolds stresses have an outer maximum while the mean velocity profile does not have an inflection point. Furthermore, in the case of flow DNS2015, Maciel, Gungor & Simens (2017) studied the coherent structures in the outer region of the large-defect part of the flow and they were not able to detect any sign of an inflectional instability. The presence or not of an inflectional instability for large-defect TBLs is still an open issue.

In the case of $\langle u^2 \rangle$ and $\langle w^2 \rangle$ (figure 7*a*,*c*), the abrupt rise of the maximum position as $H$ increases corresponds to a switch from a near-wall to an outer maximum, which is the position in the flow where the outer maximum now exceeds the near-wall maximum. Interestingly, for all flows for which such a switch can be followed (the numerical ones), the switch does not occur for the same $H$ value for $\langle u^2 \rangle$ and $\langle w^2 \rangle$. It occurs at a smaller $H$ for $\langle w^2 \rangle$ than for $\langle u^2 \rangle$. In other words, the stronger near-wall peak of $\langle u^2 \rangle$ takes more time to decay than the near-wall peak of $\langle w^2 \rangle$ in the decelerating non-equilibrium TBLs.

In the case of $\langle v^2 \rangle$ and $\langle uv \rangle$, the smoother evolutions seen in figure 7(*b*,*d*) reflect the fact that the profiles of these Reynolds stresses always have only one maximum at a time (see for instance figure 5), as opposed to $\langle u^2 \rangle$ and $\langle w^2 \rangle$ whose near-wall maximum is distinct from the outer maximum (see figure 4).

https://doi.org/10.1017/jfm.2018.193 Published online by Cambridge University Press

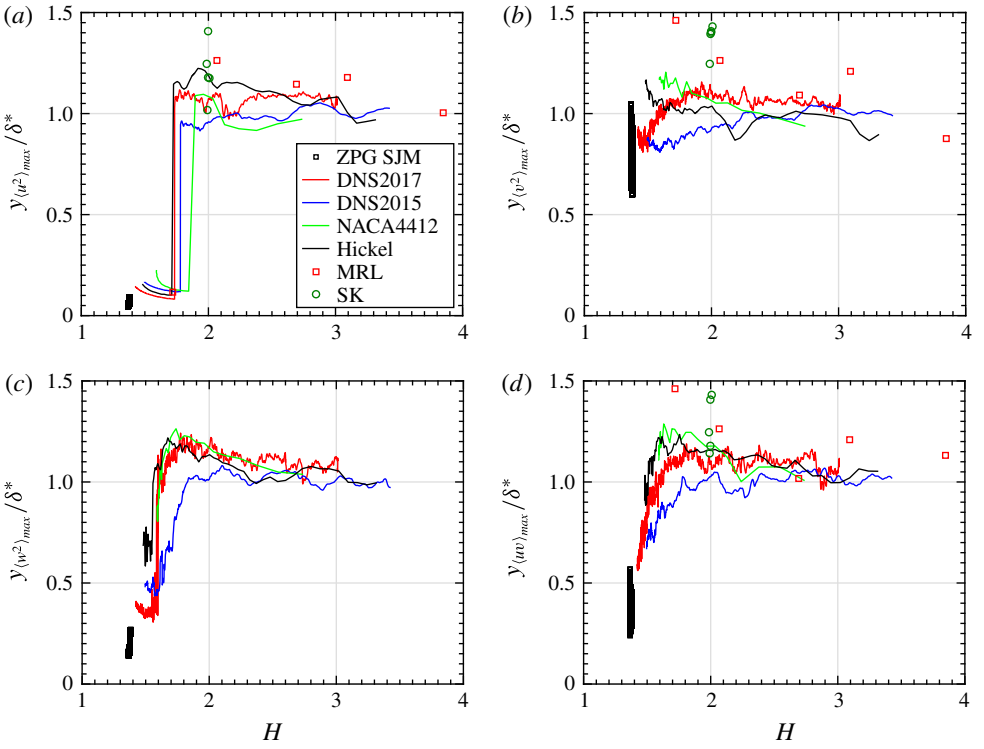



FIGURE 7. (Colour online) Wall-normal position of the maximum of the Reynolds stress components, normalized by $\delta^*$, as a function of $H$.

The fact that $\delta^*$ scales the position of the outer maximum of the Reynolds stresses raises an interesting issue. If it remains the case for higher Reynolds numbers, then these outer peaks would very slowly approach the wall as the Reynolds number increases since, as mentioned previously, $\delta^*/\delta$ slowly tends to zero as the Reynolds number tends to infinity. Furthermore, in connection with what has just been said, it is also worth mentioning that the fact that $\delta^*$ scales the position of the outer maximum of the Reynolds stresses does not mean that $\delta^*$ is the proper length scale to characterize the size of the outer region.

Now that the behaviours of the maxima of the Reynolds stresses have been assessed, these maxima can be used to demonstrate the scaling behaviour of all Reynolds stress components and for all flows. Figure 8 shows how the maximum value of the Reynolds stresses normalized with $U_{po}^2$ evolves with mean velocity defect (note that ZPG TBL data cannot be shown with $U_{po}$ as a scale). It can be seen that $U_{po}$ is indeed a scale of the Reynolds stresses for large-defect TBLs, 'large' corresponding to approximately $H > 1.8$. The scaled Reynolds stresses are of order of magnitude one. The scaled outer peaks slightly increase with $H$ for all non-equilibrium TBLs, with the exception of Hickel's flow. Similar plots for the maximum value of the Reynolds stresses normalized with $u_\tau^2$ (not shown) reveal of course an inverse trend, in the sense that $u_\tau$ is a scale of the Reynolds stresses only for small-defect TBLs, approximately for $H < 1.8$.

https://doi.org/10.1017/jfm.2018.193 Published online by Cambridge University Press

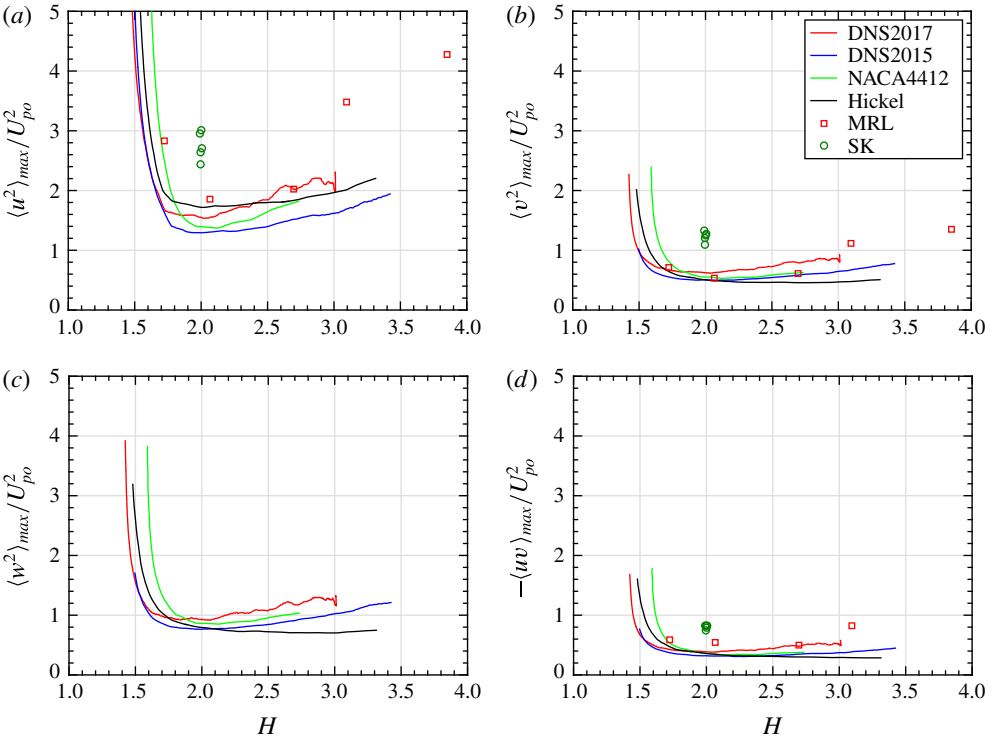



FIGURE 8. (Colour online) Maximum value of the Reynolds stresses normalized with $U_{po}^2$. Note that $U_{po} = 0$ for ZPG TBLs.

The maximum value of the Reynolds stresses normalized with $U_{zs}^2$ are presented in figure 9, where it is now possible to include also the ZPG TBL data. This figure shows that $U_{zs}$ is a scale of all Reynolds stresses for all TBLs, whatever the extent of the mean velocity defect. The Reynolds stresses scaled with $U_{zs}^2$ are of order of magnitude 0.1. The initial sharp decrease of the maximum of $\langle u^2\rangle$ seen in figure 9(*a*) corresponds to the attenuation of the near-wall peak as $H$ increases, but the near-wall peak is still higher than the outer peak in this range of low $H$ values. As seen previously with figure 6, once $H$ exceeds approximately 1.8, the maximum of $\langle u^2\rangle$ corresponds now to the outer peak. For all Reynolds stresses, the value of the outer peak scaled with $U_{zs}^2$ slightly decreases with $H$ in the five non-equilibrium flows. In the case of the two quasi-equilibrium TBLs, namely the ZPG TBL and SK flow, the maximum of the Reynolds stresses scaled with $U_{zs}^2$ decreases with Reynolds number. The only exception is $\langle -uv\rangle_{max}/U_{zs}^2$ of SK, which remains fairly constant. The behaviour of the Reynolds stresses scaled with $U_m^2$ is very similar to that of the Reynolds stresses scaled with $U_{zs}^2$ for all flows. This can be appreciated with figures 4(*c*,*d*) and 5(*c*,*d*) for flow DNS2017.

## 4. Consistent set of non-dimensional parameters

Now that the behaviour of the outer length and velocity scales is known, the incompressible, two-dimensional and Reynolds-averaged TBL equations are used to

https://doi.org/10.1017/jfm.2018.193 Published online by Cambridge University Press

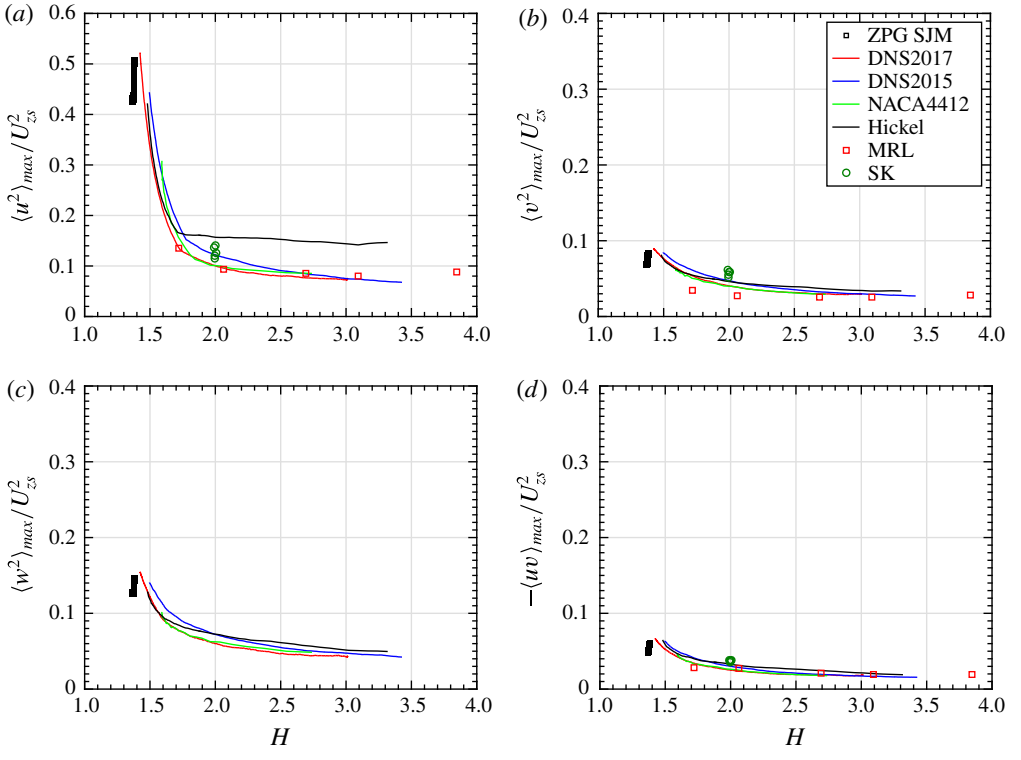



FIGURE 9. (Colour online) Maximum value of the Reynolds stresses normalized with $U_{zs}^2$.

bring out in a consistent manner the non-dimensional parameters characterizing the outer region of APG TBLs. These equations are

$$\frac{\partial U}{\partial x}+\frac{\partial V}{\partial y}=0, \tag{4.1}$$

$$0=-U\frac{\partial U}{\partial x}-V\frac{\partial U}{\partial y}-\frac{1}{\rho}\frac{\mathrm{d}p_e}{\mathrm{d}x}-\frac{\partial\langle uv\rangle}{\partial y}-\frac{\partial(\langle u^2\rangle-\langle v^2\rangle)}{\partial x}+\nu\frac{\partial^2 U}{\partial y^2}, \tag{4.2}$$

where the pressure gradient is taken at the edge of the boundary layer (index $e$). The momentum equation (4.2) is written in the format of a force balance. Equations (4.1) and (4.2) are now transformed into a single equation of motion with the following two steps. Firstly, $\partial U/\partial x$ in the streamwise momentum equation (4.2) is replaced by $-\partial V/\partial y$ from the continuity equation (4.1). Secondly, the Reynolds normal stress gradients are neglected. They are non-negligible, but small, only for very large-defect TBLs, typically very close to separation. Performing the aforementioned combination and simplification, the TBL equations are reduced to a single partial differential equation, (4.3), with no streamwise derivatives for the velocity moments – a crucial point for the analysis:

$$0=U\frac{\partial V}{\partial y}-V\frac{\partial U}{\partial y}-\frac{1}{\rho}\frac{\mathrm{d}p_e}{\mathrm{d}x}-\frac{\partial\langle uv\rangle}{\partial y}+\nu\frac{\partial^2 U}{\partial y^2}. \tag{4.3}$$

https://doi.org/10.1017/jfm.2018.193 Published online by Cambridge University Press

The non-dimensional variables are chosen as

$$\eta(x, y) = \frac{y}{L_o}, \quad x^*(x, y) = \frac{x}{L_x}, \tag{4.4a,b}$$

$$U^*(x^*, \eta) = \frac{U}{U_e}, \quad V^*(x^*, \eta) = \frac{V}{V_e}, \quad R_{12}^*(x^*, \eta) = -\frac{\langle uv \rangle}{U_o^2}, \tag{4.5a–c}$$

where generic wall-normal length scale $L_o$ and velocity scale $U_o$ of the outer region are used, for the moment, in order to retain generality.

The above non-dimensional variables have been chosen with care in order to obtain physically meaningful non-dimensional parameters. This choice deserves to be explained. Firstly, the reference velocities $U_e$, $V_e$ and $U_o$ ensure that each term in the resulting non-dimensional equation of motion (4.11) is of known order of magnitude. The resulting non-dimensional variables are normalized variables in the case of $\eta$, $x^*$, $U^*$ and $V^*$ ($\eta$, $U^*$ and $V^*$ are bounded between zero and one in the outer region), whereas $R_{12}^*$ is a scaled variable, in the sense that it retains the same order of magnitude throughout the flow regions considered. However, the constant order of magnitude of the scaled variable $R_{12}^*$ is not necessarily one. As we saw in the previous section (see figures 5, 8 and 9), results show that $-\langle uv \rangle / u_\tau^2$ and $-\langle uv \rangle / U_{po}^2$ are of order of magnitude one in their domains of validity, roughly $H < 1.8$ and $H > 1.8$, respectively. In contrast, $-\langle uv \rangle / U_{zs}^2$ and $-\langle uv \rangle / U_m^2$ are respectively of order of magnitude 0.1 and 0.01 for all types of TBL. The fact that the order of magnitude is not one in the case of $U_{zs}$ and $U_m$ has an impact on the interpretation of the non-dimensional parameters derived below, as we will see in the next section.

Secondly, by using the normalization $U^* = U/U_e$ instead of the defect formulation (scaled mean velocity defect)

$$\frac{U_e - U}{U_o}, \tag{4.6}$$

we ensure that the pressure force will not be mixed with other forces in the resulting non-dimensional equation of motion – this is a drawback of all defect formulations of the boundary layer equations, such as the equation of motion of equilibrium boundary layers and the momentum integral equation. In this manner, the resulting non-dimensional parameters will have a clear physical meaning. The normalization $U^* = U/U_e$ is nonetheless fully consistent with the mean velocity-defect scaling (4.6). This can be demonstrated with matched asymptotic expansions (Afzal 1983, 2008; Panton 2005), where the outer expansion is also usually expressed as $U/U_e$. In the present representation, assuming a fixed $x^*$, we can write the outer expansion as

$$U^*(x^*, \eta) = \frac{U}{U_e} = 1 + \gamma F_1(x^*, \eta) + \cdots, \tag{4.7}$$

where $F_1$ is the first-order function. By choosing $\gamma = U_o/U_e$ as the perturbation parameter or gauge function in the outer expansion of $U^*$, the first-order function $F_1$ is, to first order, the scaled velocity defect:

$$-F_1(x^*, \eta) \approx \frac{1}{\gamma}(1 - U^*) = \frac{U_e - U}{U_o}. \tag{4.8}$$

The scale of the velocity defect is therefore $U_o$, not $U_e$, even if $U_e$ is used as the reference value for $U$.

https://doi.org/10.1017/jfm.2018.193 Published online by Cambridge University Press

Thirdly, the $x^*$ dependence of the normalized/scaled velocity moments indicates that self-similarity is not assumed in the outer region. In other words, the scaled mean velocity-defect and Reynolds stress profiles can evolve in the streamwise direction, which is what happens in non-equilibrium TBLs, as seen in the previous section.

Finally, it is worth mentioning that in the present analysis it is not necessary to define explicitly the streamwise reference length $L_x$ because (4.3) does not include streamwise derivatives of the velocity moments. However, a streamwise reference length is necessary in order to compare different TBLs, as done in §§ 2 and 5. With the present choice of normalized variables (4.4) and (4.5), the continuity equation leads to

$$L_x(x) \propto \frac{U_e}{V_e} L_o. \tag{4.9}$$

Using a reference length of this type that implicitly depends on the variable being normalized, $x$, is however not desirable nor practicable, as explained at the beginning of § 2, where a non-local streamwise reference length $\delta_{av}$ was chosen.

Now that the non-dimensional variables have been chosen (equations (4.4) and (4.5)) and explained, equation (4.3) is expressed with them and then multiplied by $L_o/U_o^2$, which yields

$$0 = \frac{U_e V_e}{U_o^2}\left(U^*\frac{\partial V^*}{\partial \eta} - V^*\frac{\partial U^*}{\partial \eta}\right) - \frac{L_o}{\rho U_o^2}\frac{\mathrm{d}p_e}{\mathrm{d}x} + \frac{\partial R_{12}^*}{\partial \eta} + \frac{\nu}{L_o U_o}\frac{U_e}{U_o}\frac{\partial^2 U^*}{\partial \eta^2} \tag{4.10}$$

or

$$\alpha_o\left(U^*\frac{\partial V^*}{\partial \eta} - V^*\frac{\partial U^*}{\partial \eta}\right) - \beta_o + \frac{\partial R_{12}^*}{\partial \eta} + \frac{1}{Re_o}\frac{\partial^2 U^*}{\partial \eta^2} = 0. \tag{4.11}$$

Equation (4.11) is a non-dimensional form of the momentum equation that keeps constant the order of magnitude of the Reynolds shear stress gradient term in the outer region. The other terms of the equation – forces – are therefore expressed with respect to the apparent turbulent forces. Hence, the non-dimensional parameters

$$Re_o = \frac{U_o L_o}{\nu}\frac{U_o}{U_e}, \quad \beta_o = \frac{L_o}{\rho U_o^2}\frac{\mathrm{d}p_e}{\mathrm{d}x}, \quad \alpha_o = \frac{U_e V_e}{U_o^2} \tag{4.12a–c}$$

are all ratios of the order of magnitudes of two forces. The Reynolds number $Re_o$ is representative of the ratio of apparent turbulent forces to viscous forces in the outer region. It is, in other words, a local Reynolds number of large-scale turbulence in the outer region. Parameter $\beta_o$ is a pressure-gradient parameter that represents the local impact of the pressure gradient on the boundary layer in the form of a ratio of pressure forces to apparent turbulent forces. Parameter $\alpha_o$ is not a commonly used non-dimensional parameter. It reflects the ratio of inertial forces to apparent turbulent forces.

Because these three non-dimensional parameters were jointly obtained from the turbulent boundary layer equations, they form a consistent set of non-dimensional parameters that characterize the outer region of general pressure-gradient boundary layers. The flow analysis of § 5 will help further understand the significance of these parameters.

Other non-dimensional forms of the momentum equation could have been adopted, but we find that using the Reynolds shear stress gradient as the reference term is the best option because it is the only term always present in the outer region, whatever the type of TBL. For instance, using inertial forces as the reference (by dividing the terms

https://doi.org/10.1017/jfm.2018.193 Published online by Cambridge University Press

of the momentum equation by $U_eV_e$ instead of $U_o^2$) is problematic for several reasons. Firstly, one can always devise a favourable pressure-gradient TBL with $V_e = 0$, in which case the non-dimensional parameters formed with $V_e$ would all tend to infinity. A similar problem occurs if fully developed turbulent pipe and channel flows are considered (which is possible with the present analysis) since inertial forces are null in these flows. Finally, from a more minor practical viewpoint, $V_e$ is not always measured or measured accurately in laboratory or field experiments. Therefore, having $V_e$ present in all three non-dimensional parameters is not convenient. The only other option would be to use the pressure force as the reference force. However, this option is also problematic since the pressure force is absent in ZPG TBLs and in localized regions of some TBLs.

Although the non-dimensional parameters were obtained with generic scales for the sake of generality, one needs to define explicitly the scales $L_o$ and $U_o$ in order to use them. As explained in the previous section, we choose for practicality and simplicity $L_o = \delta$. If the analysis concerns only small- to moderate-defect TBLs, one possible choice of velocity scale is $U_o = u_\tau$. The resulting non-dimensional parameters are

$$Re_\tau = \frac{u_\tau \delta}{\nu}\frac{u_\tau}{U_e}, \quad \beta_\tau = \frac{\delta}{\rho u_\tau^2}\frac{\mathrm{d}p_e}{\mathrm{d}x} = \frac{\delta}{\delta^*}\beta_{RC}, \quad \alpha_\tau = \frac{U_eV_e}{u_\tau^2}. \tag{4.13a–c}$$

Note that $Re_\tau$ is not the Kármán number commonly used in the literature: $\delta^+ = u_\tau\delta/\nu$. The relationship between $\beta_\tau$ and $\beta_{RC}$ indicates that one – or both – of these two pressure-gradient parameters has to be dependent on the Reynolds number since the factor $\delta/\delta^*$ is dependent on the Reynolds number. In the similarity analysis of equilibrium TBLs of Mellor & Gibson (1966), it is implicitly assumed that $\beta_{RC}$ is independent of the Reynolds number. In contrast, Afzal (1983, 2008) performs asymptotic analyses using the inverse of $\beta_\tau$ as the chief non-dimensional parameter, which should therefore be the one that is independent of the Reynolds number. To the best of our knowledge, it has never been shown that $\beta_{RC}$ or $\beta_\tau$ is independent of the Reynolds number, and in fact it cannot be easily shown. This issue shows however that the choice of length scale is important.

Furthermore, the present analysis shows that if one wants to use $\beta_{RC}$ as the pressure-gradient parameter, then for consistency the corresponding length scale and Reynolds number are respectively $L_o = \delta^*$ and $Re_{RC} = u_\tau\delta^*/\nu(u_\tau/U_e)$. Note however that, for the reason explained in the previous section, we do not consider $\delta^*$ to be a proper outer velocity scale.

In the case of large-defect TBLs, one possible choice is $U_o = U_{po}$, yielding the following non-dimensional parameters

$$Re_{po} = \frac{U_{po}\delta}{\nu}\frac{U_{po}}{U_e}, \quad \beta_{po} = \frac{\delta}{\rho U_{po}^2}\frac{\mathrm{d}p_e}{\mathrm{d}x} = \frac{\delta}{\delta^*}, \quad \alpha_{po} = \frac{U_eV_e}{U_{po}^2}. \tag{4.14a–c}$$

It is seen that $\beta_{po}$ is simply the ratio of thicknesses $\delta/\delta^*$, without the pressure gradient appearing explicitly since $U_{po}$ itself is defined with the pressure gradient.

Finally, if one wants to analyse together all types of TBLs from small to large defect, then $U_{zs}$ or $U_m$ can be selected as the outer velocity scale $U_o$. Using $U_{zs}$ yields

$$Re_{zs} = \frac{U_{zs}\delta}{\nu}\frac{U_{zs}}{U_e}, \quad \beta_{zs} = \frac{\delta}{\rho U_{zs}^2}\frac{\mathrm{d}p_e}{\mathrm{d}x}, \quad \alpha_{zs} = \frac{U_eV_e}{U_{zs}^2} \tag{4.15a–c}$$

while using $U_m$ yields

$$Re_m = \frac{U_m\delta}{\nu}\frac{U_m}{U_e}, \quad \beta_m = \frac{\delta}{\rho U_m^2}\frac{\mathrm{d}p_e}{\mathrm{d}x}, \quad \alpha_m = \frac{U_eV_e}{U_m^2}. \tag{4.16a–c}$$

https://doi.org/10.1017/jfm.2018.193 Published online by Cambridge University Press

## 5. Analysis of the flows

The various flows are now analysed with the non-dimensional parameters defined in the previous section, that is, those defined by (4.13)–(4.16). The first two objectives here are to better understand these parameters and to determine under what conditions, depending on the scales used, they retain their meaning. The last objective is to show that these non-dimensional parameters allow us to characterize and compare TBLs with different pressure distributions.

Figure 10(*a–d*) shows the streamwise evolution of the pressure-gradient parameters $\beta_\tau$, $\beta_{po}$, $\beta_{zs}$ and $\beta_m$ for the different flows. It was demonstrated in the previous section that these pressure-gradient parameters should represent the ratio of the order of magnitude of the pressure force to the order of magnitude of the apparent turbulent force in the outer region:

$$O\left(\frac{\mathrm{d}p_e}{\mathrm{d}x}\right) \Big/ O\left(\rho\frac{\partial\langle uv\rangle}{\partial y}\right). \tag{5.1}$$

Figure 10(*e*) shows directly this ratio in the form of the pressure force over the maximum of the Reynolds shear stress gradient in the outer region – note that the momentum balance of flow DNS2015 was studied in detail by Gungor *et al.* (2016). If we focus first on figure 10(*e*), we see that the ratio of forces remains fairly constant for flow SK, a result that is expected since dynamic equilibrium is by essence the definition of an equilibrium TBL. The non-equilibrium nature of the five other APG TBLs is reflected by the important streamwise variation of the ratio of forces. For four of the present non-equilibrium TBLs – DNS2017, DNS2015, Hickel and MRL – the importance of the pressure force with respect to the turbulent force decreases in the outer region as the velocity defect increases in the large-defect zones of these flows (downstream). Flow NACA4412 behaves differently in that the dominance of the pressure force keeps increasing all the way to the airfoil trailing edge.

In figure 10(*a*,*b*), $\beta_\tau$ and $\beta_{po}$ are shown for the whole selected streamwise region of each flow – the same one used in the previous figures – even if these pressure-gradient parameters are not valid over the whole region of the APG boundary layers. For instance, figure 10(*e*) indicates that $\beta_\tau$ no longer represents the order of magnitude of the ratio of pressure to turbulent forces in the outer region when $H$ exceeds approximately 1.6, and this is true for all APG TBLs studied here, including the quasi-equilibrium TBL of SK (the point where $H = 1.6$ is illustrated with + signs in figure 10(*a*,*b*), for the flows obtained numerically). The fact that $\beta_\tau$ loses its meaning as the ratio of pressure to turbulent forces for $H > 1.6$ is consistent with the fact that $u_\tau$ is no longer a scale of the mean velocity defect and Reynolds stresses for roughly $H > 1.8$, as shown in § 3. In the case of MRL flow, $\beta_\tau$ has the meaning of the ratio of the orders of magnitude of pressure and turbulent forces only for the first data point. Note that $\beta_{RC}$, shown in figure 1(*c*), behaves similarly to $\beta_\tau$. The meaning of $\beta_{RC}$ and $\beta_\tau$ is discussed further below.

One cannot normally use $\beta_{po}$ for small-defect TBLs since $U_{po}$ is not a valid outer velocity scale for very small pressure gradients. A comparison of figure 10(*b*) and figure 10(*e*) shows that, in the small-defect zones of these flows (upstream segments of the non-equilibrium TBLs), $\beta_{po}$ retains the correct order of magnitude of the ratio of pressure to turbulent forces, but the streamwise evolutions and magnitude ranking between flows are wrong. Nonetheless, $\beta_\tau$ (when it is valid) and $\beta_{po}$ are the ones that give the right order of magnitude of the ratio of forces. In order to reflect the correct order of magnitude, $\beta_{zs}$ and $\beta_m$ have to be multiplied by 10 and 100, respectively, as

https://doi.org/10.1017/jfm.2018.193 Published online by Cambridge University Press

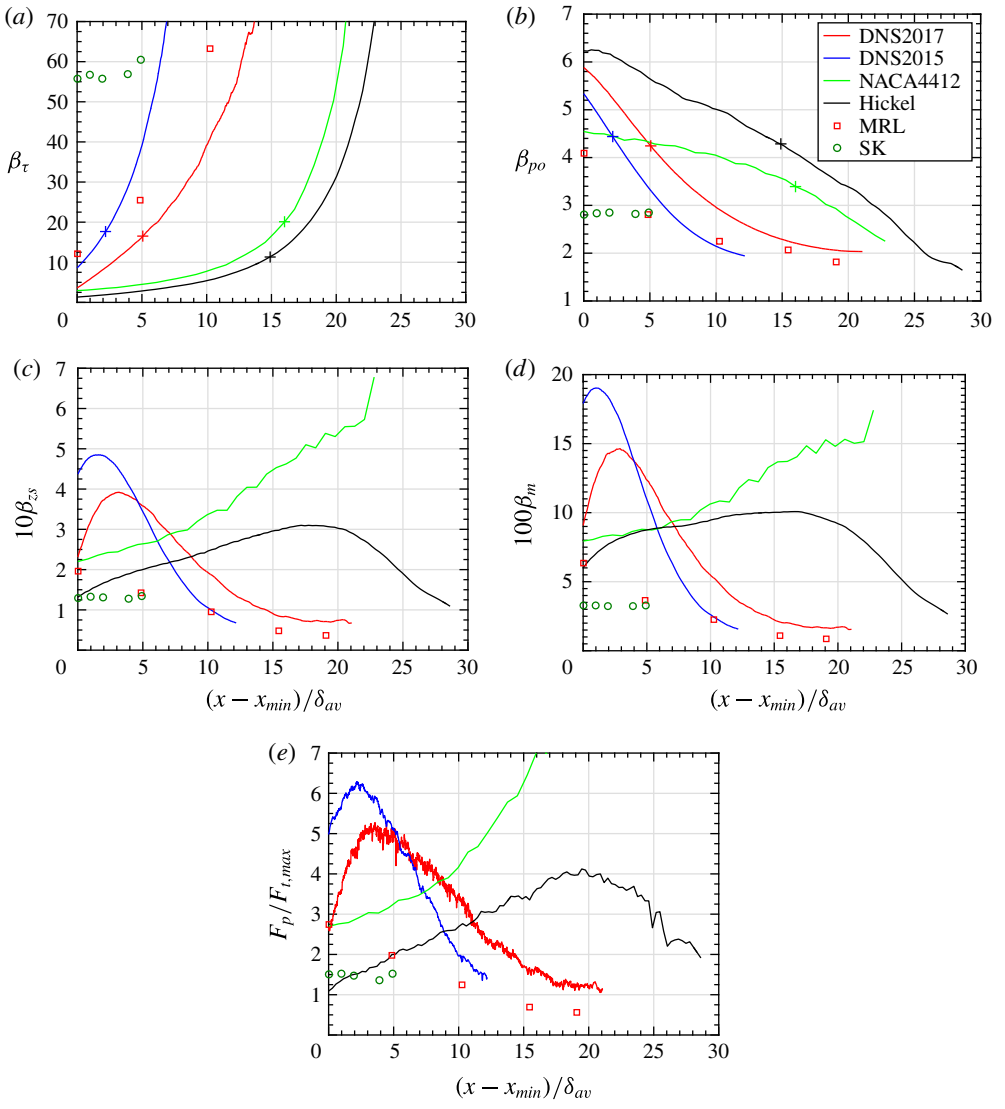



FIGURE 10. (Colour online) Outer region pressure-gradient parameter $\beta_o$ with $U_o$ taken as (*a*) $u_\tau$, (*b*) $U_{po}$, (*c*) $U_{zs}$ and (*d*) $U_m$. Note that $\beta_o = 0$ for ZPG TBLs. The + signs on the lines mark the positions where $H = 1.6$. (*e*) Ratio of the pressure force $F_p$ to the maximum Reynolds shear stress gradient in the outer region $F_{t,max}$.

is done in figure 10(*c*,*d*) – we use powers of 10 since this is an order-of-magnitude analysis. This stems from the fact that the scaled Reynolds shear stress gradient – $\partial R_{12}^*/\partial\eta$ in equation (4.11) – is of order of magnitude one in the outer region if $U_o$ equals $u_\tau$ or $U_{po}$ in the domains of validity of these velocity scales (roughly $H < 1.8$ and $H > 1.8$, respectively) and of order of magnitude 0.1 and 0.01 for all types of TBLs if $U_o$ equals $U_{zs}$ or $U_m$. These orders of magnitude can be appreciated from figure 11 in the case of $U_{po}$ and $U_{zs}$, and indirectly from the Reynolds shear stress profiles of figure 5 for flow DNS2017.

https://doi.org/10.1017/jfm.2018.193 Published online by Cambridge University Press

In § 3, we emphasized and showed that the outer velocity scales only reveal the order of magnitude of the mean velocity defect and the Reynolds stresses – they do not reveal scale invariance or universal similarity. Consequently, it was expected that the pressure-gradient parameter would only reflect the order of magnitude of the ratio of pressure to turbulent forces in the outer region, not a precise value of this ratio. However, quite to our astonishment, a comparison of figure 10(*c*) with figure 10(*e*) clearly indicates that $\beta_{zs}$ represents very well this ratio. Thus $\beta_{zs}$ permits one to follow the streamwise evolution of the ratio of pressure to turbulent forces, and to compare it between flows. Such a good correspondence is impressive and unexpected. As we will see below, the same is also true for $\alpha_{zs}$ and $Re_{zs}$. These three parameters can therefore be used to follow the streamwise evolution of the streamwise mean momentum balance – in a global sense – in the outer region.

The second best representation of the ratio of pressure to turbulent forces is given by $\beta_m$, which is less accurate than $\beta_{zs}$ in representing the upstream evolution and magnitude of the ratio of forces for flow Hickel, and the downstream part of flow NACA4412. In figure 10(*b*), if we focus on the zones where $\beta_{po}$ should be valid (right of the + signs for the numerical flows, last four data points for MRL, and all data points for SK), we see that $\beta_{po}$ is much less accurate than $\beta_{zs}$ and $\beta_m$ in representing the streamwise evolutions and magnitudes of the ratio of forces. In fact, $\beta_{po}$ gives the wrong streamwise evolution and magnitude for flow NACA4412.

The explanation for these results lies in the fact that $U_{zs}^2$ scales extremely well the amplitude of the Reynolds shear stress gradient in the outer region. This can be appreciated with figure 11, where a comparison is made between the maximum value of the Reynolds shear stress gradient normalized with $U_{po}^2$ and $U_{zs}^2$. For all flows and all velocity-defect conditions, this maximum value follows almost a single curve when scaled with $U_{zs}^2$ and expressed as a function of $H$ (figure 11*b*). Moreover, it is almost constant, only varying between 0.5 and 1.0 (with $U_{zs}^2$ divided by 10). Consequently, with $U_o = U_{zs}$, the non-dimensional Reynolds shear stress gradient in (4.11) has an almost constant maximum amplitude in the outer region. Therefore $\beta_{zs}$ gives an almost exact representation of the ratio of pressure force to maximum turbulent force.

Figures 11(*c*) and 11(*d*) are equivalent to figures 11(*a*) and 11(*b*) respectively, but with the streamwise position as abscissa instead of $H$. They are only shown to allow a direct comparison with figures 10 and 12. Figures 11(*a*) and 11(*b*) are more useful, since they reveal the scaling trend as a function of the mean velocity defect.

The pressure-gradient parameters that involve the wall shear stress, the Rotta–Clauser pressure-gradient parameter $\beta_{RC}$ and $\beta_\tau$, change meaning when the mean velocity defect is important. As we have seen in § 3, with figure 6 as an example, $\beta_{RC}$ can reflect – but in some cases only, as explained below – the state of a TBL from small defect to large defect. In other words, $\beta_{RC}$ and $\beta_\tau$ are indicators of the cumulative impact (local and upstream history) of the pressure gradient on the boundary layer. However, they are imperfect indicators of such an impact because they comprise a parameter that is independent of history effects: the local value of the pressure gradient. In the case of the present non-equilibrium TBLs, $\beta_{RC}$ and $\beta_\tau$ reflect well the cumulative impact of the pressure gradient but this is only because these are flows with a monotonic increase of $\beta_{RC}$ (monotonic increase of $H$). An example of a situation where $\beta_{RC}$ and $\beta_\tau$ fail to reflect the cumulative impact of the pressure gradient is a TBL that is still responding to an upstream pressure gradient although the pressure gradient has returned to zero, hence $\beta_{RC} = \beta_\tau = 0$. This example shows that the shape factor $H$ is a better indicator of the cumulative impact (local and upstream history) of the pressure gradient on the boundary layer. Moreover, its

https://doi.org/10.1017/jfm.2018.193 Published online by Cambridge University Press

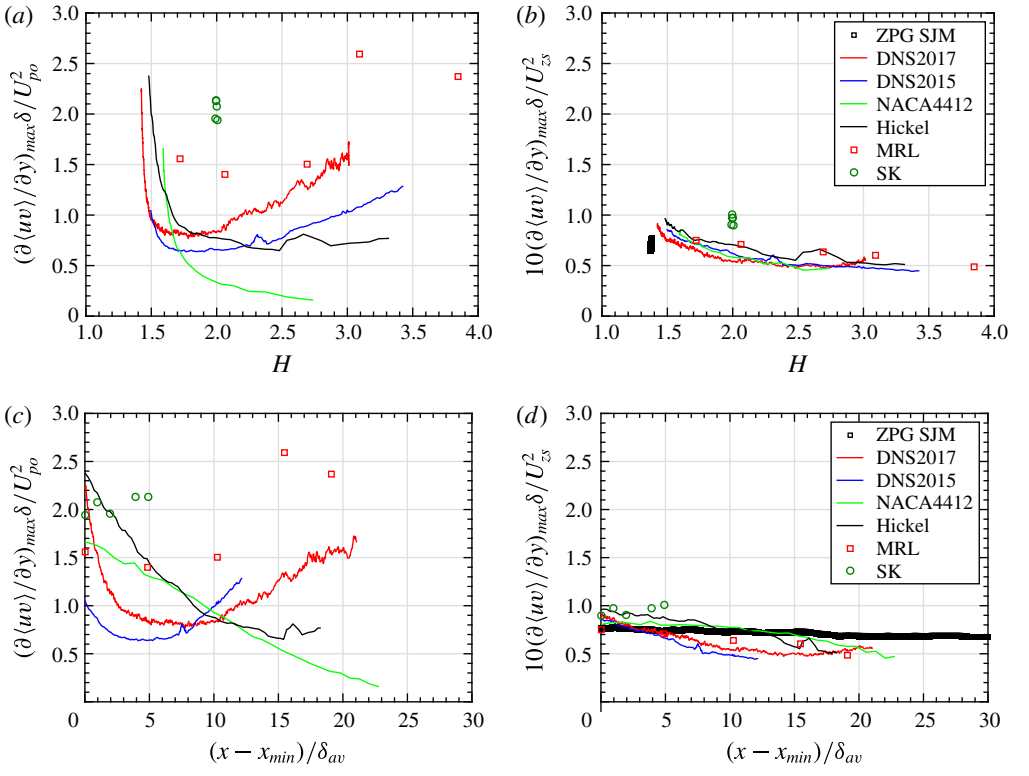



FIGURE 11. (Colour online) Maximum value of the Reynolds shear stress gradient in the outer region normalized with (*a*) $U_{po}^2$ and (*b*) $U_{zs}^2$ as a function of $H$. Same ordinates for (*c*,*d*) but as a function of $(x_{min}-x)/\delta_{av}$.

definition does not assume any choice of scales, contrary to $\beta_{RC}$ and the Rotta–Clauser defect shape factor $G$.

The issue of the physical meaning of $\beta_{RC}$ is important since it is probably the most widely used pressure-gradient parameter. To the authors' knowledge, the only other situation where $\beta_{RC}$ has a clear meaning is in the context of equilibrium TBLs. In this context, Mellor & Gibson (1966), Schlichting & Gersten (2000) and Maciel *et al.* (2006*b*) rewrite the ordinary differential equation of motion of equilibrium TBLs in order to bring out $\beta_{RC}$ as one of the similarity parameters. However, it is important to insist that, even in this case, $\beta_{RC}$ does not come out naturally as one of the similarity parameters; much in the same manner as in the present analysis $\beta_o$ clearly does not have to be $\beta_{RC}$.

The inertial parameter is now discussed. Figure 12(*a–d*) shows the streamwise evolution of the inertial parameters $\alpha_\tau$, $\alpha_{po}$, $\alpha_{zs}$ and $\alpha_m$ for the flows for which $V$ was available. These parameters should represent the ratio of the order of magnitude of the inertial force (streamwise mean momentum advection) to the order of magnitude of the apparent turbulent force in the outer region:

$$O\left(U\frac{\partial U}{\partial x}+V\frac{\partial U}{\partial y}\right)\Big/O\left(\frac{\partial\langle uv\rangle}{\partial y}\right). \tag{5.2}$$

Figure 12(*e*) shows directly this ratio in the form of the maximum mean momentum advection over the maximum Reynolds shear stress gradient in the outer region. Note

https://doi.org/10.1017/jfm.2018.193 Published online by Cambridge University Press

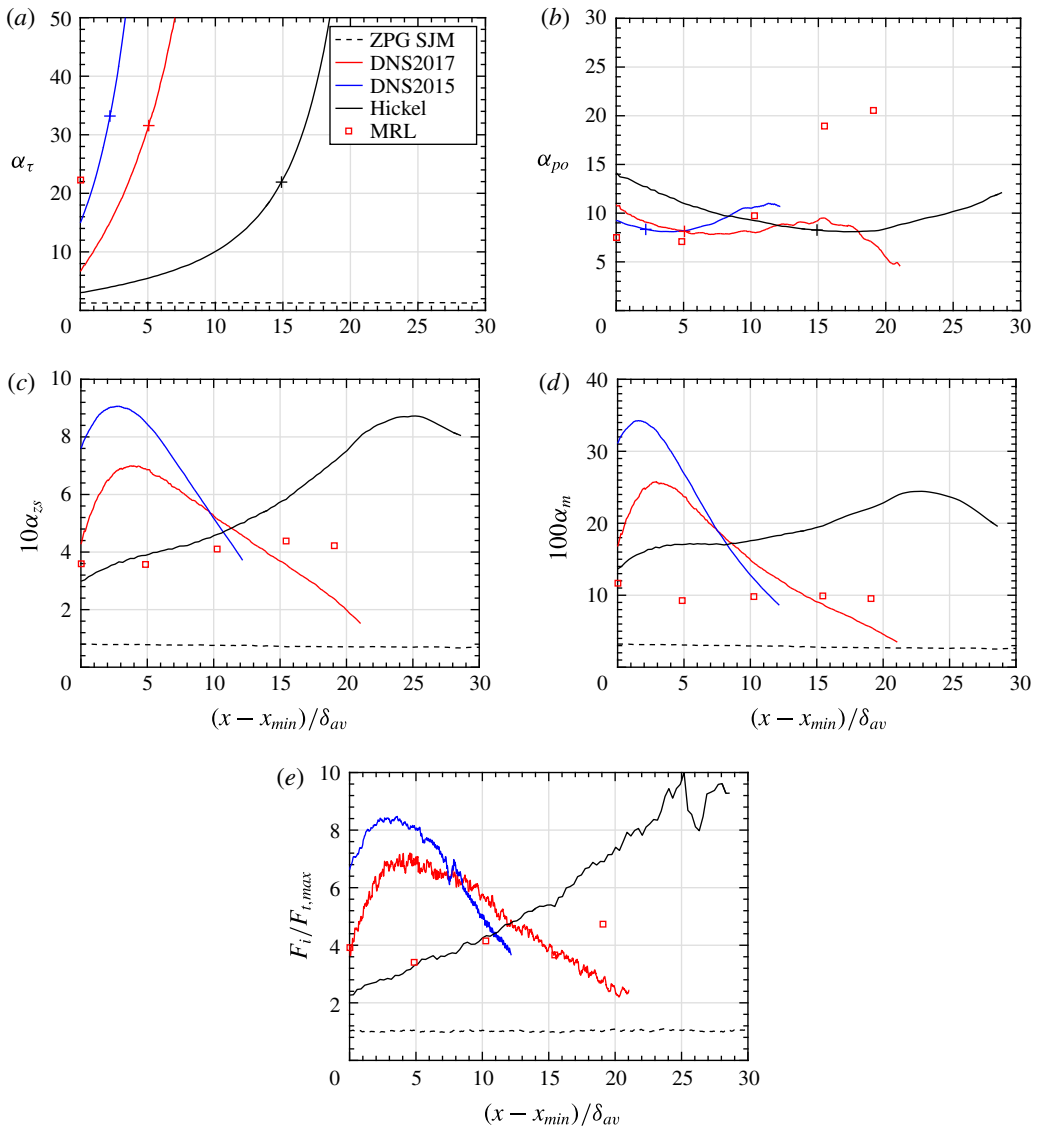



FIGURE 12. (Colour online) Outer region parameter $\alpha_o$ with $U_o$ taken as (*a*) $u_\tau$, (*b*) $U_{po}$, (*c*) $U_{zs}$ and (*d*) $U_m$. The + signs on the lines mark the positions where $H = 1.6$. (*e*) Ratio of the maximum inertial force $F_{i,max}$ to the maximum Reynolds shear stress gradient $F_{t,max}$ in the outer region.

that, in order to reduce considerably the uncertainty in the computation of these maxima, the profiles of $U$, $V$ and $\langle uv \rangle$ were smoothed with cubic splines before computing the derivatives.

Similarly to what was obtained for the pressure-gradient parameter, we see that $\alpha_{zs}$ represents very well the streamwise evolution of the ratio of the inertial force to the apparent turbulent force in the outer region. Again, this is quite an impressive result. The other inertial parameters, $\alpha_\tau$, $\alpha_{po}$ and $\alpha_m$, represent the order of magnitude of the ratio of forces (when they are valid) but nothing more. As for the pressure-gradient

https://doi.org/10.1017/jfm.2018.193 Published online by Cambridge University Press

parameters, $\alpha_\tau$ no longer reflects this order of magnitude when roughly $H > 1.6$. This is the case for all data points of flow SK and the last four data points of MRL.

We see from figure 12(*e*) (or figure 12*c*) that inertia tends to dominate the apparent turbulent force in the APG TBLs, in contrast to the situation in the ZPG TBL, where the two forces have about the same magnitude. Like the ratio of pressure to turbulent forces, the streamwise evolution of the ratio of inertia to turbulent forces varies considerably from one APG TBL to another.

Figure 13 presents the streamwise evolution of the Reynolds numbers $Re_\tau$, $Re_{po}$, $Re_{zs}$ and $Re_m$ for the different flows. Recall that these Reynolds numbers should represent the ratio of the order of magnitude of the Reynolds shear stress gradient (apparent turbulent force) to the order of magnitude of the viscous force in the outer region:

$$O\left(\rho\frac{\partial\langle uv\rangle}{\partial y}\right)\Big/O\left(\mu\frac{\partial^2 U}{\partial y^2}\right). \tag{5.3}$$

Figure 13(*e*) presents this ratio in the form of the maximum Reynolds shear stress gradient over the maximum viscous shear stress gradient in the outer region. Again, in order to reduce considerably the uncertainty in the computation of these maxima, the profiles of $U$ and $\langle uv\rangle$ were smoothed with cubic splines before computing the derivatives. Even so, the uncertainty in the value of $\partial^2 U/\partial y^2$ is high, in particular for the two experimental databases. Consequently, the results presented in figure 13(*e*) have to be analysed with caution due to their high uncertainty. That being said, these results indicate that, as expected, the SK flow has the highest turbulent Reynolds number in the outer region by far, followed by MRL. DNS2017 and Hickel flows appear to be globally at a slightly higher outer Reynolds number than DNS2015, NACA4412 and ZPG SJM.

Despite the aforementioned uncertainty, we can probably conclude that the order of magnitude of the ratio of the maximum Reynolds shear stress gradient to the maximum viscous force in the outer region is well represented by $Re_{po}$, $Re_{zs}$ and $Re_m$. However, $Re_{po}$ overestimates this ratio of forces in the downstream part of flow NACA4412. Note that the streamwise evolution of $\beta_{po}$ was also wrong for NACA4412. It is therefore possible that we have incorrect $\mathrm{d}p_e/\mathrm{d}x$ values for this flow even though these values have been checked. As for $Re_{zs}$ and $Re_m$, they seem to overestimate the force ratio in all non-equilibrium TBLs when the velocity defect becomes important. However, they allow the force ratio of the ZPG TBL to be compared with that of the other flows, something that $Re_{po}$ cannot do.

As with the other two non-dimensional parameters, $Re_\tau$ loses its meaning as the ratio of turbulent to viscous forces for $H > 1.6$. This is the case for all data points of flow SK and the last four data points of MRL. For all non-equilibrium TBLs, the loss of significance of $Re_\tau$ is reflected by the fact that $Re_\tau$ starts decreasing as the mean velocity defect increases, while $Re_{po}$, $Re_{zs}$ and $Re_m$ clearly indicate that the outer region Reynolds number $Re_o$ keeps increasing.

The most commonly used local boundary layer Reynolds number is $Re_\theta$, shown in figure 1(*a*), and already discussed in § 2. Performing an analysis similar to that done in § 4, we can show that $Re_\theta$ is also the ratio of apparent turbulent forces to viscous forces in the outer region, if we use $\theta$ as the reference wall-normal length $L_o$ and $U_e$ as the reference velocity for the Reynolds shear stress. However, as discussed

https://doi.org/10.1017/jfm.2018.193 Published online by Cambridge University Press

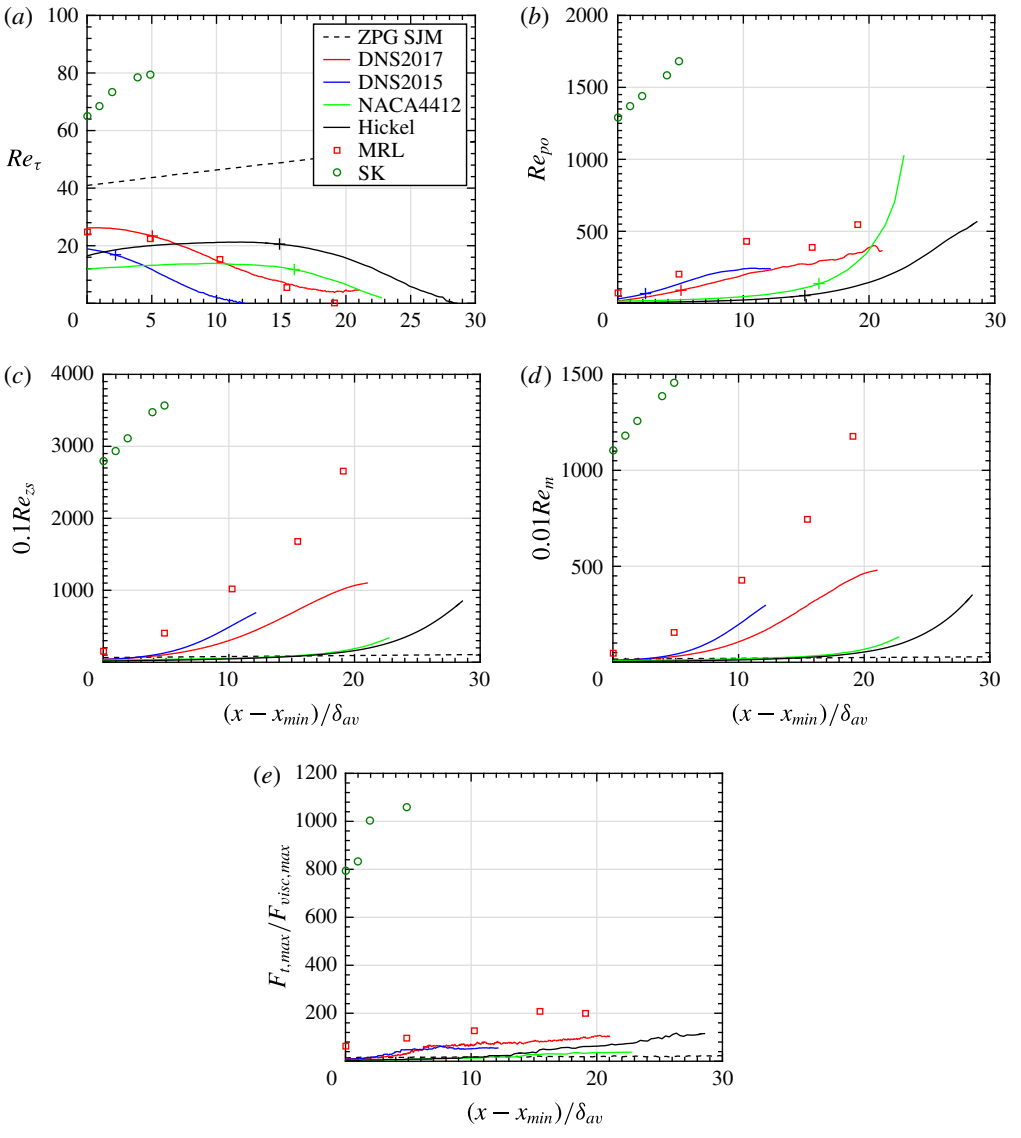



FIGURE 13. (Colour online) Outer region Reynolds number $Re_o$ with $U_o$ taken as (*a*) $u_\tau$, (*b*) $U_{po}$, (*c*) $U_{zs}$ and (*d*) $U_m$. Note that $Re_{po} = 0$ for ZPG TBLs. The + signs on the lines mark the positions where $H = 1.6$. (*e*) Ratio of the maximum Reynolds shear stress gradient $F_{t,max}$ to the maximum viscous shear stress gradient $F_{visc,max}$ in the outer region.

previously, $\theta$ is not a proper outer length scale and $U_e$ is not an outer velocity scale of the Reynolds shear stress. For these reasons, a comparison of $Re_\theta$ (figure 1*a*) with the force ratio (figure 13*e*) shows that $Re_\theta$ does not give the correct order of magnitude of this ratio. Moreover, it overestimates the force ratio of the small-defect flows/zones (such as the ZPG TBL) in comparison to the large-defect flows/zones. The streamwise evolutions are however well represented in the large-defect flows/zones.

https://doi.org/10.1017/jfm.2018.193 Published online by Cambridge University Press

## 6. Conclusions

Although we have used in this paper ideas and knowledge coming from similarity theories of turbulent boundary layers, we have deliberately put aside the theoretical developments behind these theories to start afresh, from basic ideas of fluid mechanics. In this manner, we have established a consistent framework to treat and analyse the outer region of general pressure-gradient TBLs. As a first step, a selection of outer velocity and length scales for the mean velocity defect and Reynolds stresses have been presented and discussed. We have argued in particular why the displacement and momentum thicknesses are not appropriate scales of the thickness of the outer region – we also showed that the displacement thickness scales perfectly the position of the outer maximum of the Reynolds stresses, but this is a different scaling. More importantly, it is emphasized that length and velocity scales do not need to reveal scale invariance (universal similarity) of the mean velocity-defect and Reynolds stress profiles since, as the present results clearly show, it does not exist in the case of non-equilibrium pressure-gradient TBLs. Therefore, in the context of general pressure-gradient TBLs, the only property that is required of a scale is that it reflects the order of magnitude of the scaled variable for all types of flows or flow regions considered.

Using this scale definition, we have demonstrated the range of validity of the four selected velocity scales with the help of six APG TBL databases and a ZPG one. The selected velocity scales are the friction velocity $u_\tau$, the pressure-gradient velocity $U_{po}$, the Zagarola–Smits velocity $U_{zs}$ and the mixing-layer-type velocity $U_m$. The range of validity of these scales is best expressed in terms of the shape factor $H$ since its definition does not assume any *a priori* choice of scales, contrary to the Rotta–Clauser pressure-gradient parameter $\beta_{RC}$ and the Rotta–Clauser defect shape factor $G$. The results show that the approximate range of validity of $u_\tau$ is $H < 1.8$ and that of $U_{po}$ is $H > 1.8$. These limits are only approximate because they depend on Reynolds number and upstream history. The results also show that, as expected from previous studies, $U_{zs}$ and $U_m$ are valid outer velocity scales for all types of TBLs, from small to very large velocity defect.

The major contribution of this paper is to provide a consistent set of non-dimensional parameters characterizing the outer region of general pressure-gradient turbulent boundary layers – moreover, each of these parameters has a clear physical meaning. This was achieved by performing a non-dimensional analysis of the continuity and momentum equations with the following determinant choices:

(i) The analysis does not rely on any similarity assumption. It therefore applies to all types of pressure-gradient TBLs. In other words, it is not specific to equilibrium TBLs or to canonical turbulent wall flows.

(ii) The momentum equation is not written with the mean velocity-defect formulation, which is what is usually done in the literature for the outer region. The advantage in doing so is that we keep only one term in the momentum equation that involves the pressure gradient (or external velocity gradient) instead of several. In this manner, we are able to isolate each type of force in the momentum equation. With a mean velocity-defect formulation, the force terms become intermingled.

(iii) We have used a generic length scale $L_o$ and velocity scale $U_o$ of the outer region to perform the analysis. The resulting non-dimensional parameters are therefore not 'contaminated' by an *a priori* choice of velocity and length scales.

(iv) The reference velocities used in the analysis were chosen in such a manner that each term in the resulting non-dimensional equation of motion is of known order of magnitude.

https://doi.org/10.1017/jfm.2018.193 Published online by Cambridge University Press

(v) By choosing a form of the equation of motion that does not involve streamwise derivatives of the velocity moments, it was not necessary to define a streamwise reference length. As explained in the paper, determining such a reference length is not a trivial issue. If it was present in the analysis, it would have complicated the meaning of the non-dimensional parameters.

In terms of the generic scales $L_o$ and $U_o$, the non-dimensional parameters found are the pressure-gradient parameter $\beta_o = L_o/(\rho U_o^2)\,\mathrm{d}p_e/\mathrm{d}x$, the Reynolds number $Re_o = U_o L_o/\nu(U_o/U_e)$ and the inertia parameter $\alpha_o = U_e V_e/U_o^2$, where $U_e$ and $V_e$ are respectively the streamwise and wall-normal components of mean velocity at the boundary layer edge. They form a consistent and rigorous set of parameters to treat and analyse general pressure-gradient TBLs. They represent the ratio of the magnitudes of two types of forces in the outer region, using the Reynolds shear stress gradient (apparent turbulent force) as the reference force: inertia to apparent turbulent forces for $\alpha_o$, pressure to apparent turbulent forces for $\beta_o$, and apparent turbulent to viscous forces for $Re_o$.

The results clearly show that the best representation of these three ratios of forces in the outer region is obtained with the set composed of $\beta_{zs}$, $\alpha_{zs}$ and $Re_{zs}$ – that is, when $U_o = U_{zs}$ and $L_o = \delta$. In fact, to our surprise, the representation is so accurate with $\beta_{zs}$ and $\alpha_{zs}$ that it is possible to follow the corresponding force ratios in all the flows, not just the order of magnitude of these ratios (the representation is less accurate for $Re_{zs}$ but still better than an order-of-magnitude representation). The explanation for such a surprising result lies in the fact that the amplitude of the Reynolds shear stress gradient in the outer region is almost scale-invariant when scaled with $U_{zs}^2$. Consequently and impressively, the streamwise evolution of the streamwise mean momentum balance in the outer region can be followed – in a global sense – with $\beta_{zs}$, $\alpha_{zs}$ and $Re_{zs}$. This cannot be achieved with $\beta_o$, $Re_o$ and $\alpha_o$ expressed with $u_\tau$ or $U_{po}$, and only imperfectly with $U_m$.

However, if $U_{zs}^2$ is used as the outer scale of the Reynolds shear stress ($U_o = U_{zs}$), then it should be divided by a factor 10 so that $\beta_{zs}$, $\alpha_{zs}$ and $Re_{zs}$ give the correct order of magnitude of the ratio of forces – we use powers of 10 since this is an order-of-magnitude analysis; an exact numerical factor does not exist. Similarly, if $U_m^2$ is used as the outer scale of the Reynolds shear stress, then it should be divided by a factor 100. In other words, by dividing $U_{zs}^2$ and $U_m^2$ by a factor 10 and 100, respectively, the Reynolds shear stress gradient scaled with these velocity scales is of order of magnitude one, for all types of turbulent boundary layers.

Furthermore, the meaning of the Rotta–Clauser pressure-gradient parameter $\beta_{RC} = (\delta^*/\tau_w)\,\mathrm{d}p_e/\mathrm{d}x$ has been clarified since it is equal to $\beta_o$ when $L_o = \delta^*$ and $U_o = u_\tau$. The present results show that it loses its meaning as a local pressure-gradient parameter for $H > 1.6$ because it implies $U_o = u_\tau$. It can be conjectured that it also loses its meaning as a local pressure-gradient parameter for very large Reynolds numbers since it implies $L_o = \delta^*$ whereas $\delta^*/\delta$ tends to zero in the limit of an infinite Reynolds number. For $H > 1.6$, $\beta_{RC}$ and $\beta_\tau$ can become qualitatively similar to the shape factor $H$, in that they reflect the cumulative impact (upstream history) of the pressure gradient on the boundary layer. However, this is not the case for all non-equilibrium TBLs. We have also argued that there is actually no theoretical reason why $\beta_{RC}$ should be the preferred pressure-gradient parameter, not even in the context of equilibrium turbulent boundary layers.

Now that sets of consistent scales and governing parameters have been established, the next step would be to devise a complete theory of arbitrary pressure-gradient turbulent boundary layers, inspired for instance by the existing similarity theories.

https://doi.org/10.1017/jfm.2018.193 Published online by Cambridge University Press

However, as mentioned in the introduction, this requires high-quality near-wall data at high Reynolds numbers and covering a wide spectrum of pressure-gradient conditions. Fortunately, such data are starting to appear both experimentally and numerically. The non-dimensional parameters derived in this paper can help design flow cases in a consistent and rigorous manner, since they provide the streamwise evolution of all ratios of forces in the outer region.

**Acknowledgements**

The authors of the various databases used in this study are gratefully acknowledged for sharing their data. A.G.G. and Y.M. were supported respectively by ITU-BAP and NSERC of Canada. The computation of DNS2017 was made possible by a generous grant of computer time from Compute Canada. T.W. is grateful for the financial support of New Mexico Institute of Mining and Technology and Los Alamos National Laboratory.

## REFERENCES

ABE, H. 2017 Reynolds-number dependence of wall-pressure fluctuations in a pressure-induced turbulent separation bubble. *J. Fluid Mech.* **833**, 563–598.

AFZAL, N. 1983 Analysis of a turbulent boundary layer subjected to a strong adverse pressure gradient. *Intl J. Engng Sci.* **21** (6), 563–576.

AFZAL, N. 2008 Turbulent boundary layer with negligible wall stress. *Trans. ASME J. Fluids Engng* **130** (5), 051205.

ANGELE, K. P. & MUHAMMAD-KLINGMANN, B. 2006 PIV measurements in a weakly separating and reattaching turbulent boundary layer. *Eur. J. Mech. (*B*/Fluids)* **25** (2), 204–222.

BOBKE, A., VINUESA, R., ÖRLÜ, R. & SCHLATTER, P. 2017 History effects and near equilibrium in adverse-pressure-gradient turbulent boundary layers. *J. Fluid Mech.* **820**, 667–692.

CLAUSER, F. H. 1954 The turbulent boundary layer in adverse pressure gradient. *J. Aero. Sci.* **21**, 91–108.

CLAUSER, F. H. 1956 The turbulent boundary layer. In *Advances in Applied Mechanics* (ed. H. L. Dryden & Th. von Karman), vol. 4, pp. 1–51. Elsevier.

COLES, D. E. 1956 The law of the wake in the turbulent boundary layer. *J. Fluid Mech.* **1** (02), 191–226.

COLES, D. E. 1969 The young persons guide to the data. In *1968 AFOSR-IFP-Stanford Conference Computation of Turbulent Boundary Layers: Compiled Data*, vol. 2, pp. 1–45. Thermosciences Division, Stanford University.

COLES, D. E. & HIRST, E. (Eds) 1969 *1968 AFOSR-IFP-Stanford Conference Computation of Turbulent Boundary Layers: Compiled Data*, vol. 2. Thermosciences Division, Stanford University.

CUVIER, C., SRINATH, S., STANISLAS, M., FOUCAUT, J. M., LAVAL, J. P., KHLER, C. J., HAIN, R., SCHARNOWSKI, S., SCHRDER, A., GEISLER, R. *et al.* 2017 Extensive characterisation of a high Reynolds number decelerating boundary layer using advanced optical metrology. *J. Turbul.* **18** (10), 929–972.

DURBIN, P. A. & BELCHER, S. E. 1992 Scaling of adverse-pressure-gradient turbulent boundary layers. *J. Fluid Mech.* **238**, 699–722.

ELSBERRY, K., LOEFFLER, J., ZHOU, M. D. & WYGNANSKI, I. 2000 An experimental study of a boundary layer that is maintained on the verge of separation. *J. Fluid Mech.* **423**, 227–261.

GUNGOR, A. G., MACIEL, Y., SIMENS, M. P. & GUNGOR, T. 2017 Direct numerical simulation of a non-equilibrium adverse pressure gradient boundary layer up to $Re_\theta = 8000$. In *16th European Turbulence Conference, Stockholm, Sweden*, European Mechanics Society.

GUNGOR, A. G., MACIEL, Y., SIMENS, M. P. & SORIA, J. 2014 Analysis of a turbulent boundary layer subjected to a strong adverse pressure gradient. *J. Phys.: Conf. Ser.* **506**, 012007.

https://doi.org/10.1017/jfm.2018.193 Published online by Cambridge University Press

GUNGOR, A. G., MACIEL, Y., SIMENS, M. P. & SORIA, J. 2016 Scaling and statistics of large-defect adverse pressure gradient turbulent boundary layers. *Intl J. Heat Fluid Flow* **59**, 109–124.

HARUN, Z., MONTY, J. P., MATHIS, R. & MARUSIC, I. 2013 Pressure gradient effects on the large-scale structure of turbulent boundary layers. *J. Fluid Mech.* **715**, 477–498.

HICKEL, S. & ADAMS, N. A. 2008 Implicit LES applied to zero-pressure-gradient and adverse-pressure-gradient boundary-layer turbulence. *Intl J. Heat Fluid Flow* **29** (3), 626–639.

HOSSEINI, S. M., VINUESA, R., SCHLATTER, P., HANIFI, A. & HENNINGSON, D. S. 2016 Direct numerical simulation of the flow around a wing section at moderate Reynolds number. *Intl J. Heat Fluid Flow* **61**, 117–128.

INDINGER, T., BUSCHMANN, M. T. & GAD-EL HAK, M. 2006 Mean-velocity profile of turbulent boundary layers approaching separation. *AIAA J.* **44**, 2465–2474.

INOUE, M., PULLIN, D. I., HARUN, Z. & MARUSIC, I. 2013 LES of the adverse-pressure gradient turbulent boundary layer. *Intl J. Heat Fluid Flow* **44**, 293–300.

KADER, B. A. & YAGLOM, A. M. 1978 Similarity treatment of moving-equilibrium turbulent boundary layers in adverse pressure gradients. *J. Fluid Mech.* **89** (02), 305–342.

KITSIOS, V., SEKIMOTO, A., ATKINSON, C., SILLERO, J. A., BORRELL, G., GUNGOR, A. G., JIMNEZ, J. & SORIA, J. 2017 Direct numerical simulation of a self-similar adverse pressure gradient turbulent boundary layer at the verge of separation. *J. Fluid Mech.* **829**, 392–419.

KLINE, S. J., COLES, D. E. & HIRST, E. (Eds) 1969 *1968 AFOSR-IFP-Stanford Conference Computation of Turbulent Boundary Layers: Methods, Predictions, Evaluation, and Flow Structure*, vol. 1. Thermosciences Division, Stanford University.

KNOPP, T., BUCHMANN, N. A., SCHANZ, D., EISFELD, B., CIERPKA, C., HAIN, R., SCHRDER, A. & KHLER, C. J. 2015 Investigation of scaling laws in a turbulent boundary layer flow with adverse pressure gradient using PIV. *J. Turbul.* **16** (3), 250–272.

KNOPP, T., REUTHER, N., NOVARA, M., SCHULEIN, E., SCHANZ, D., SCHRDER, A. & KHLER, C. J. 2017 Investigation of a turbulent boundary layer flow at high Reynolds number using particle-imaging and implications for RANS modeling. In *Tenth International Symposium on Turbulence and Shear Flow Phenomena (TSFP10), Chicago, USA*, Darmstadt University of Technology.

LEE, J. H. & SUNG, H. J. 2009 Structures in turbulent boundary layers subjected to adverse pressure gradients. *J. Fluid Mech.* **639**, 101–131.

LOGDBERG, O., ANGELE, K. & ALFREDSSON, P. H. 2008 On the scaling of turbulent separating boundary layers. *Phys. Fluids* **20**, 075104.

LUDWIEG, H. & TILLMANN, W. 1949 Untersuchungen über die wandschubspannung in turbulenten reibungsschichten. *Ing.-Arch.*; translated as Investigations of the wall-shearing stress in turbulent boundary layers, *NACA Tech. Mem. No.* 1285, 1950, **17**.

MACIEL, Y., GUNGOR, A. G. & SIMENS, M. 2017 Structural differences between small and large momentum-defect turbulent boundary layers. *Intl J. Heat Fluid Flow* **67**, 95–110.

MACIEL, Y., ROSSIGNOL, K. S. & LEMAY, J. 2006*a* A study of a turbulent boundary layer in stalled-airfoil-type flow conditions. *Exp. Fluids* **41** (4), 573–590.

MACIEL, Y., ROSSIGNOL, K. S. & LEMAY, J. 2006*b* Self-similarity in the outer region of adverse-pressure-gradient turbulent boundary layers. *AIAA J.* **44** (11), 2450–2464.

MARQUILLIE, M., LAVAL, J.-P. & DOLGANOV, R. 2008 Direct numerical simulation of a separated channel flow with a smooth profile. *J. Turbul.* **9** (1).

MCDONALD, H. 1969 The effect of pressure gradient on the law of the wall in turbulent flow. *J. Fluid Mech.* **35** (02), 311–336.

MELLOR, G. L. & GIBSON, D. M. 1966 Equilibrium turbulent boundary layers. *J. Fluid Mech.* **24** (02), 225–253.

MELNIK, R. E. 1989 An asymptotic theory of turbulent separation. *Comput. Fluids* **17** (1), 165–184.

NA, Y. & MOIN, P. 1998 Direct numerical simulation of separated turbulent boundary layer. *J. Fluid Mech.* **374**, 379–405.

PANTON, R. L. 2005 Review of wall turbulence as described by composite expansions. *Appl. Mech. Rev.* **58** (1), 1–36.

https://doi.org/10.1017/jfm.2018.193 Published online by Cambridge University Press

PERRY, A. E., BELL, J. B. & JOUBERT, P. N. 1966 Velocity and temperature profiles in adverse pressure gradient turbulent boundary layers. *J. Fluid Mech.* **25** (02), 299–320.

PERRY, A. E. & SCHOFIELD, W. H. 1973 Mean velocity and shear stress distributions in turbulent boundary layers. *Phys. Fluids* **16** (12), 2068–2074.

RAHGOZAR, S. & MACIEL, Y. 2012 Statistical analysis of low- and high-speed large-scale structures in the outer region of an adverse pressure gradient turbulent boundary layer. *J. Turbul.* **13**, 1–24.

ROTTA, J. 1950 Uber die theorie der turbulenten grenzschichten. *Mitt. Max Planck Inst. Strmungsforsch., Göttingen*; translated as On the theory of turbulent boundary layers, *NACA Tech. Mem. No.* 1344, 1953, **1**.

SATO, M., ASADA, K., NONOMURA, T., KAWAI, S. & FUJII, K. 2017 Large-eddy simulation of NACA 0015 airfoil flow at Reynolds number of $1.6 \times 10^6$. *AIAA J.* **55** (2), 673–679.

SCHLICHTING, H. & GERSTEN, K. 2000 *Boundary-Layer Theory*, 8th edn. Springer.

SILLERO, J., JIMÉNEZ, J. & MOSER, R. 2013 One-point statistics for turbulent wall-bounded flows at Reynolds numbers up to $\delta^+ \approx 2000$. *Phys. Fluids* **25**, 105102.

SKÅRE, P. E. & KROGSTAD, P. Å. 1994 A turbulent equilibrium boundary layer near separation. *J. Fluid Mech.* **272**, 319–348.

SKOTE, M. & HENNINGSON, D. S. 2002 Direct numerical simulation of separated turbulent boundary layer. *J. Fluid Mech.* **471**, 107–136.

SPALART, P. R. & WATMUFF, J. H. 1993 Experimental and numerical study of a turbulent boundary layer with pressure gradients. *J. Fluid Mech.* **249**, 337–371.

TOWNSEND, A. A. 1956*a* *The Structure of Turbulent Shear Flow*. Cambridge University Press.

TOWNSEND, A. A. 1956*b* The properties of equilibrium boundary layers. *J. Fluid Mech.* **1** (06), 561–573.

TOWNSEND, A. A. 1961 Equilibrium layers and wall turbulence. *J. Fluid Mech.* **11** (01), 97–120.

VINUESA, R., BOBKE, A., ÖRLÜ, R. & SCHLATTER, P. 2016 On determining characteristic length scales in pressure-gradient turbulent boundary layers. *Phys. Fluids* **28** (5), 055101.

YAJNIK, K. S. 1970 Asymptotic theory of turbulent shear flows. *J. Fluid Mech.* **42** (2), 411–427

https://doi.org/10.1017/jfm.2018.193 Published online by Cambridge University Press